J. Fluid Mech. (1992), *vol.* 244, *pp.* 257–288

Weakly nonlinear theory of regular meanders

By G. SEMINARA AND M. TUBINO
Istituto di Idraulica, Università di Genova, Via Montallegro 1, 16145 Genova, Italy

(Received 17 October 1991 and in revised form 13 April 1992)

Flow and bed topography in a regular sequence of meanders is shown to be strongly influenced by nonlinear effects within a fairly wide range of aspect ratios of the channel and meander wavenumbers. This finding is associated with the behaviour of meanders as nonlinear resonators in a neighbourhood of the resonance conditions discovered by Blondeaux & Seminara (1985). A weakly nonlinear approach valid for relatively small measures of channel curvature and within a neighbourhood of the resonant conditions displays all the typical features of nonlinear resonators, including non-uniqueness of the channel response. The nonlinear structure of forced bars close to resonance is also shown to be related to that of nonlinear free steady bars spatially developing in a straight channel from a non-uniform initial condition. Finally we show how to reconcile the intrinsic nonlinearity of the near-resonant channel response with traditional bend stability theories. Some comparison with a systematic set of experimental observations of Colombini, Tubino & Whiting (1990) provides qualitative support for the present theory but also suggests that strongly nonlinear effects may play a non-negligible role for fairly small values of channel curvature. The main implication of this work is the clear need to revisit the literature on the modelling of flow and bed topography in river meanders, which is mostly based on linear theories.

1. Introduction

Modelling flow and bed topography in meandering channels has long attracted the attention of scientists in the fields of fluvial engineering and fluvial geomorphology. Motivation for this study comes from its relevance both to the solution of several practical problems of river engineering and to the understanding of some basic mechanisms involved in the process of formation and development of river meanders.

The present paper analyses flow and bed topography in a regular sequence of meanders, each characterized by a curvature distribution described by the well-known 'sine generated curve' of Langbein & Leopold (1966). This viewpoint, very commonly employed in the literature, is considered as the basis of a fundamental step towards the understanding of the formation of the variety of meandering patterns occurring in nature. It is known that their degree of regularity may vary considerably (see Ferguson 1975). However, the availability of a sound model for flow and bed topography in a regular sequence of meanders, besides its intrinsic relevance, seems to be an appropriate basis for future investigation of the origin of irregular patterns of river meanders.

Recent efforts of various scientists have been successful in substantiating some reasonable lines of attack to the 'regular' problem described above, by approaches sufficiently sophisticated to pick up the main physical processes involved in the phenomenon, but still simple enough to provide a manageable tool for analytical

investigation. In fact the works of Rozovskii (1957), Engelund (1974), Kalkwijk & de Vriend (1980), Ikeda, Parker & Sawai (1981), Johannesson & Parker (1989), Tubino & Seminara (1990) among others, have suggested the suitability of quasi two-dimensional models of the flow field, i.e. two-dimensional de Saint-Venant equations modified to account for the dispersive effect of the helical secondary flow induced by channel curvature on the transport of longitudinal momentum. The above equations, supplemented by the continuity equation of the sediment and by some constitutive equation describing the dynamics of sediment motion on sloping boundaries, provide a closed set of equations which exhibit a rich variety of solutions.

The picture emerging from theoretical investigations (see Seminara & Tubino 1989 for a recent review), along with experimental and field observations, suggests that rivers behave as nonlinear dynamical systems and exhibit most of their classical features.

In the absence of curvature the dynamical character of these systems is related to the occurrence of bottom instability. The latter may operate at different spatial scales based on channel width (alternating bars), on flow depth (dunes, antidunes, ridges) or on a smaller scale (ripples). In particular, alternating-bar instability, widely investigated in the 1970s at a linear level, occurs for sufficiently wide channels and leads to the development of large-scale bedforms, i.e. sediment waves migrating at typical speeds of metres per day. This perturbed configuration has been shown to bifurcate from the unperturbed uniform flow and bed topography in the form of a supercritical Hopf bifurcation (Colombini, Seminara & Tubino 1987).

A second source of non-equilibrium of rivers is bank erosion which may lead to the development of curvature of the channel axis. The latter forces the formation of steady sequences of pools and riffles (often called 'point bars') which follow the development of the meander pattern, generally slightly out of phase with respect to curvature. Blondeaux & Seminara (1985) showed that the forcing effect of curvature in a periodic sequence of meanders may lead to the resonant excitation of a class of alternating bars characterized by vanishing growth rate, i.e. steady and non-amplifying. The above finding was based on a linear theory of flow and bed topography in river meanders, hence it predicted an infinite peak of the linear response at resonance. Since the above work appeared, the occurrence of resonance was confirmed by Seminara & Tubino (1985), Johannesson & Parker (1989) and Odgaard (1989) (see Seminara & Tubino's 1991 discussion) on the basis of different linear models. The basic requirements for resonance to occur are that for given averaged flow and sediment characteristics, the dimensionless meander wavenumber λ and the undisturbed width-to-depth ratio β of the channel coincide with the marginal values (λ_R, β_R) corresponding to steady non-amplifying alternating bars.

The above resonance conditions have been associated with meander formation (through so called 'bend theories') as they lead to a peak of bottom stress and thus to maximum potential bank erosion and bend amplification. The latter line of reasoning is based on various simplifying assumptions which will be recalled in §7.

A dual viewpoint, which turns out to be strongly related to the idea of resonance, has been pursued in the 1980s by the Dutch School (see Struiksma *et al.* 1985). Basically the idea is to associate meander formation with the planimetric growth of steady bottom perturbations which develop spatially within the initially straight channel starting from some perturbed initial condition in space. Since the marginal conditions for spatially growing perturbations coincide with the resonant conditions of Blondeaux & Seminara (1985) the above two approaches appear to be strongly related.

In the present contribution we intend to remove one of the basic restrictions of both the above approaches: the assumption of linearity, i.e. the restriction to small-amplitude perturbations of flow and bed topography. It will be shown that the nonlinear theory of near-resonant meanders is related to the nonlinear theory of spatially growing disturbances. Nonlinearity turns out to damp both the infinite peak in the response detected by linear theory of resonance and the indefinite exponential growth of spatially growing bars. Furthermore the nonlinear amplitude equation governing the response of near-resonant meanders is found to consist of a homogeneous part which coincides with the amplitude equation governing the spatial development of steady bars and a non-homogeneous part describing the forcing effect of curvature. In other words it is confirmed at a nonlinear level that at resonance curvature forces a natural response of the channel consisting of steady bars.

The relevance of the above results appears to be related to an important question which originally motivated the present investigation. Indeed the occurrence of resonance and the need to account for nonlinearity in order to remove the infinite response predicted by linear theory makes one wonder how wide is the range of meander wavenumbers and aspect ratios of the channel cross-section where the effects of resonance are significant. Knowledge of the behaviour of classical nonlinear resonators, like that associated with Duffing equation (see, for instance, Thompson & Stewart 1986, p. 72) suggests the possibility that nonlinearity may widen the resonant range and lead to further interesting features like non-uniqueness of the nonlinear response. The analysis performed in this paper, which is based on a perturbation expansion in a neighbourhood of resonance, suggests that this is indeed the case, i.e. nonlinear resonant meanders exhibit a response which may be non-unique and differs significantly from the linear response within a fairly wide range of wavenumbers of practical significance.

The implication of the latter results (which will have to be confirmed by strongly nonlinear calculations valid within a wider range of wavenumbers) is the need to revisit the literature on the modelling of flow and bed topography in river meanders, which is mostly based on linear theories. In particular the above findings set the basis for an investigation of the development of finite-amplitude meanders where the controlling mechanism of the generation of higher (third) harmonics of the fundamental meander frequency is associated with flow nonlinearities, a mechanism distinct from the one based on geometric nonlinearities investigated by Parker, Diplas & Akiyama (1983).

In order to check the consistency and correctness of the above picture Colombini, Tubino & Whiting (1990) performed a detailed and systematic experimental investigation of bed topography in meandering channels for a wide range of values of meander wavenumbers and width-to-depth ratios, including the resonant values. Though the present weakly nonlinear approach is strictly valid for very small channel curvature and experimental results reveal the presence of a non-negligible contribution of higher harmonics, nevertheless various theoretical predictions seem to be confirmed.

The problem is formulated in §2. Section 3 briefly recapitulates previous results of linear theory of resonant meanders and linear theory of spatially growing bars. In §4 the nonlinear development of spatially growing bars is shown to lead to an amplitude equation of Landau-Stuart type which allows us to predict the occurrence of a supercritical Hopf bifurcation. In §5 we determine the nonlinear amplitude equation governing the response of river meanders in a neighbourhood of resonance. Section

6 is devoted to investigating the solutions of the latter amplitude equation and their stability. In §7 we discuss some implications of the present results on bend theory of river meanders. Section 8 is devoted to some comparison of the present results with the experimental findings of Colombini *et al.* (1990). Finally, a discussion of the main results of the paper and of their validity limits is contained in the last section.

2. Formulation of the problem

The theoretical investigation of flow and bed topography in meandering channels poses a complex mathematical problem which requires some model of a three-dimensional turbulent flow field and of the mechanics of sediment transport on sloping boundaries.

The approach we employ herein is similar to the one recently used by Tubino & Seminara (1990) (hereinafter referred to as TS) to investigate the interaction between free migrating alternating bars and forced steady bars in meandering channels. We summarize below the basic ideas of the model and refer the reader to the above paper for further details.

We consider wide curved channels with gently sloping banks. More precisely, the width of the channel ($2B^*$) is assumed to greatly exceed the average flow depth D_0^* and the curvature of the wetted boundary is taken to be small enough for transverse turbulent diffusion of longitudinal momentum to be negligible. Furthermore we assume the channel axis to have constant slope S and be described by a so-called 'sine generated curve' whereby we can write (see figure 1)

$$R_0^*/r_0^* = r_0^{-1}(s) = e_1 + \text{c.c.} = \exp(\mathrm{i}\lambda s) + \text{c.c.}, \qquad (1a\text{–}c)$$

$$\lambda = \lambda^* B^*, \quad s = s^*/B^*, \qquad (1d, e)$$

with R_0^* twice the radius of curvature at the bend apex, r_0^* the local radius of curvature, λ^* the meander wavenumber, and s^* the curvilinear longitudinal coordinate (here, and throughout the paper, an asterisk denotes a dimensional quantity and c.c. is complex conjugate).

A convenient orthogonal coordinate system to describe flow and bed topography in such channels is (s^*, n^*, z^*), such that n^* is horizontal and z^* is directed upward. The metric coefficients of the latter system are readily found to be (see TS, p. 133)

$$h_s = 1 + n^*/r_0^*, \quad h_n = 1, \quad h_z = 1, \qquad (2a\text{–}c)$$

having neglected the very small torsion of the channel axis and assumed the curvature of the channel axis to be positive when the centre of curvature lies along the negative n^*-axis.

The simplest approach to modelling flow and bed topography in meandering channels is based on two-dimensional depth-average model where account is properly taken of the fact that the secondary flow induced by channel curvature exhibits a 'helical' component characterized by zero depth average. In the process of depth-averaging the three-dimensional Reynolds equation the latter component leads to some 'dispersive' terms which play a non-negligible role (see Kalkwijk & de Vriend 1980). Following the latter authors and TS we then assume the following decomposition of the velocity field

$$u = u_0(z)\, U(s,n), \quad v = \nu[\Gamma_0(z;\lambda)\, e_1 + \text{c.c.}]\, U(s,n) + u_0(z)\, V(s,n), \qquad (3a, b)$$

$$(u, U, v, V,) = 1/U_0^*\,(u^*, U^*, v^*, V^*), \quad n = n^*/B^*, \quad z = z^*/D_0^*, \qquad (3c\text{–}e)$$

where (u^*, v^*) and (U^*, V^*) are local and depth-averaged longitudinal and transverse components of velocity respectively, U_0^* and D_0^* are averaged speed and depth of the

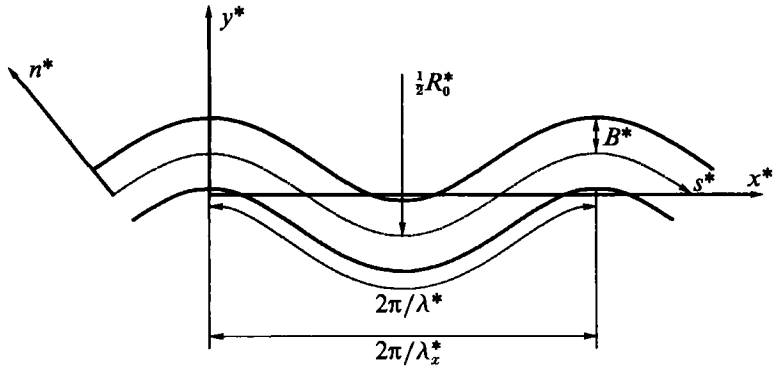

FIGURE 1. Sketch of the channel.

uniform unperturbed flow, $u_0(z)$ is the vertical structure of the unperturbed uniform velocity distribution, and $\Gamma_0(z)$ is the vertical structure of the helical component of secondary flow as it emerges from fully three-dimensional linear models (see Seminara & Tubino 1989). Linearity of the latter models is expressed by the assumption of small typical curvature ratio of the channel, hence

$$\nu \equiv B^*/R_0^* \ll 1 \tag{4}$$

Though the decomposition (3*a*, *b*) has been previously discussed in TS it may be useful to recall some of its main features.

(i) The helical component of the secondary flow scales with $\nu' = D_0^*/R_0^*$ rather than ν. However, in a meandering channel convective terms and metric coefficients involve B^* rather then D_0^* as a spatial scale. Hence the parameter ν naturally arises. In the analysis below we choose ν as perturbation parameter and let $\nu \to 0$ with the ratio B^*/D_0^* fixed. It is then convenient to write the helical component in terms of ν rather than ν' with the dispersive terms taken to be a factor D_0^*/B_0^* smaller than the original ones.

(ii) The validity of decomposition (3*a*, *b*) is only approximate. In fact, results from three-dimensional model (see Seminara & Tubino 1989) show that both vertical distributions associated with the depth-averaged components of u and v coincide with $u_0(z)$ at a linear level, and neglecting the effect of longitudinal convection. It is reasonable to expect that the analysis will not be greatly affected by the above simplification. In fact, longitudinal convection is fully accounted for in the depth-averaged model and is only neglected in the evaluation of 'dispersive' effects which are fairly small (see TS, figure 4).

By substituting from (3*a*, *b*) into the three-dimensional Reynolds equations written in the present coordinate system, performing depth integration and neglecting transverse turbulent diffusion of longitudinal momentum we find the following differential equations for the depth-averaged components of the flow field:

$$UU_{,s}+VU_{,n}+H_{,s}+\frac{\beta\tau_s}{D}=-\nu\mathscr{R}(s)\left[n\left(\frac{\beta\tau_s}{D}+VU_{,n}\right)+UV\right]-\nu\mathscr{R}_1(s)\frac{1}{D}(U^2D)_{,n}+O(\nu^2), \tag{5}$$

$$UV_{,s}+VV_{,n}+H_{,n}+\beta\frac{\tau_n}{D}=-\nu\mathscr{R}(s)\left[n\left(VV_{,n}+H_{,n}+\frac{\beta\tau_n}{D}\right)-U^2\right]$$

$$-\nu\mathscr{R}_1(s)\left\{\frac{1}{D}[(DU^2)_{,s}+2(UDV)_{,n}]\right\}-\nu(\mathrm{i}\lambda k_1 e_1+\mathrm{c.c.})\,U^2+O(\nu^2), \tag{6}$$

$$(DU)_{,s}+(DV)_{,n}=-\nu\mathscr{R}(s)\,[VD+n(DV)_{,n}], \tag{7}$$

$$(F_0^2H-D)_{,t}+(Q_{s,s}+Q_{n,n})=-\frac{\nu\mathscr{R}(s)}{1+\nu n\mathscr{R}(s)}(Q_n-nQ_{s,s}), \tag{8}$$

where the local flow depth D^*, the free-surface elevation H^*, the components of bottom shear stress (τ_s^*,τ_n^*) and of sediment flow rate (Q_s^*,Q_n^*) in the longitudinal and transverse directions, and the time t^*, are made dimensionless in the form:

$$(H^*,D^*)=D_0^*(F_0^2H,D),\quad (\tau_s^*\,\tau_n^*)=\rho U_0^{*2}(\tau_s,\tau_n), \tag{9a, b}$$

$$(Q_s^*,Q_n^*)=d_s^*\left\{\left(\frac{\rho_s}{\rho}-1\right)gd_s^*\right\}^{\frac{1}{2}}(Q_s,Q_n),\quad t^*=\frac{B^*}{U_0^*\,Q_0}t. \tag{9c, d}$$

Herein ρ_s and d_s^* are density and diameter of the sediment modelled as uniform, ρ is water density, g is gravity, and F_0 is the Froude number of the uniform unperturbed flow.

Furthermore, β is the width ratio and Q_0 is a dimensionless parameter defined as

$$\beta=\frac{B^*}{D_0^*},\quad Q_0=\frac{d_s^*((\rho_s/\rho-1)\,gd_s^*)^{\frac{1}{2}}}{(1-p)\,D_0^*\,U_0^*} \tag{10a, b}$$

with p bed porosity; and

$$\mathscr{R}(s)=e_1+\text{c.c.},\quad \mathscr{R}_1(s)=k_1e_1+\text{c.c.} \tag{11a, b}$$

where the parameter k_1 arises from the velocity decomposition (3a, b) and is plotted versus the grain relative roughness for given values of the meander wavenumber λ in figure 4(a) of TS.

Notice that in the governing differential system (5)–(8) the possibility of an unsteady response of bottom topography is preserved; however, the coexistence of free migrating alternating bars and forced point bars is excluded in the present analysis. The work of TS allows us to state that such conditions are met provided the curvature ratio ν exceeds some threshold value ν_{th} which depends on meander wavenumber for given values of the unperturbed Shields stress and grain relative roughness. Plots of ν_{th} as a function of λ are given in TS.

The differential system (5)–(8) must be supplemented by some appropriate constitutive equations relating bottom stresses and sediment transport rate to flow characteristics, appropriate account being taken of the effect of the helical component of secondary flow and of the deviation of the direction of sediment transport from the direction of average bottom stress under the gravitational effect on transverse slope. Following TS we then write

$$\tau=(\tau_s,\tau_n)=[U,V+\nu U(k_4e_1+\text{c.c.})]\,(U^2+V^2)^{\frac{1}{2}}C, \tag{12a}$$

$$k_4=[\Gamma_{0,z}/u_{0,z}]_{z=F_0^2H-D}, \tag{12b}$$

where C is a friction coefficient which is given the logarithmic form

$$C^{-\frac{1}{2}}=6+2.5\ln\left(\frac{D}{2.5d_s}\right) \tag{12c}$$

when the unperturbed bottom is assumed to be plane, and in Engelund & Hansen's (1967) form

$$\left(\frac{\theta}{\theta'C}\right)^{\frac{1}{2}}=6+2.5\ln\left(\frac{\theta'}{2.5\theta}\frac{D}{d_s}\right),\quad \theta'=0.06+0.4\theta^2 \tag{12d, e}$$

when the unperturbed bottom is assumed to be dune-covered. Herein θ and d_s denote dimensionless Shields stress and grain roughness respectively, defined as

$$\theta = \frac{|\tau^*|}{(\rho_s - \rho) g d_s^*}, \quad d_s = \frac{d_s^*}{D_0^*} \tag{13a, b}$$

We also write

$$\boldsymbol{Q} = (Q_{\tau_1}, Q_{\tau_2}, Q_v) = (\cos\delta, \sin\delta, 0)\,\Phi \tag{14}$$

where Φ is the intensity of sediment transport, $\hat{\boldsymbol{\tau}}_1$ is the unit vector in the direction of the intersection between the plane locally tangent to the bottom and the plane (s^*, z^*), $\hat{\boldsymbol{v}}$ is the unit vector in the direction normal to the bottom and $\hat{\boldsymbol{\tau}}_2$ is the unit vector in the direction orthogonal to $\hat{\boldsymbol{\tau}}_1$ and $\hat{\boldsymbol{v}}$.

The components Q_{τ_1} and Q_{τ_2} are found to be related to the longitudinal and transverse components Q_s and Q_n through

$$Q_s = Q_{\tau_1}\left[1 - \frac{1}{2}\left(\frac{\eta_{,s}}{\beta(1+\nu n\mathscr{R}(s))}\right)^2\right] - Q_{\tau_2}\frac{\eta_{,s}\eta_{,n}}{\beta^2(1+\nu n\mathscr{R}(s))} \tag{15a}$$

$$Q_n = Q_{\tau_2}\left[1 - \frac{1}{2}\left(\frac{\eta_{,n}}{\beta}\right)^2\right] \tag{15b}$$

where $\eta = (F_0^2 H - D)$ is the dimensionless local bottom elevation, and fourth-order terms in the products between the longitudinal and transverse slopes have been neglected. We point out that downslope gravitational effects retained in (15*a*, *b*) are very small and, though formally included in the analysis, do not in practice affect the solution. Also notice that the effect of variation of longitudinal slope on the direction and intensity of sediment transport is neglected herein.

The angle δ is expressed in terms of angle χ between the bottom stress and the τ_1-direction through the well-established linear relationship (see Ikeda 1982; Parker 1984)

$$\sin(\delta) = \sin(\chi) - \frac{r}{\beta\theta^{\frac{1}{2}}}\eta_{,n} \tag{16}$$

with r an empirical coefficient ranging between 0.3 and 0.6.

Finally, the intensity of sediment transport is expressed through equilibrium relationships. More precisely we employ Meyer-Peter & Muller formula in the form given by Chien (1956)

$$\Phi = 8(\theta - \theta_{cr})^{\frac{3}{2}}, \quad \theta_{cr} = 0.047 \tag{17a, b}$$

in the plane case, and Engelund & Hansen's (1967) formula

$$\Phi = 0.05 C^{-1}\theta^{\frac{5}{2}} \tag{17c}$$

in the dune case, having assumed sediment to be mainly transported as bed load.

Note that (12) and (17) are essentially equivalent to an assumption of local equilibrium of turbulence structure and sediment transport. The appropriate boundary and integral conditions to be associated with the above formulation are

$$V = Q_n = 0 \quad (n = \pm 1), \tag{18a, b}$$

$$\int_{-1}^{1} UD\,\mathrm{d}n = 2, \tag{19a}$$

$$\int_0^{2\pi/\lambda}\int_{-1}^{1} [F_0^2(H - H_0) - (D-1)]\,\mathrm{d}n\,\mathrm{d}s = 0, \tag{19b}$$

with H_0 the dimensionless free-surface elevation of the uniform unperturbed flow, which express the requirements of impermeability of channel banks to flow and

sediment (18), constant flow discharge (19a), and constant averaged reach slope (19b).

3. Linear theory of resonant meanders and spatially growing bars: a review

Let us now consider the response of flow and bed topography to curvature in channels satisfying the conditions (1a) and (4), ignoring the possible presence of migrating (free) bars. We take advantage of the 'weak curvature' assumption and, following Blondeaux & Seminara (1985), expand the solution in powers of the curvature ratio ν in the form:

$$(U, V, H, D) = (1, 0, H_0, 1) + \nu[(U_1, V_1, H_1, D_1)\, e_1 + \text{c.c.}] + O(\nu^2). \tag{20}$$

Hence we assume that perturbations with respect to the basic uniform flow are periodic in the longitudinal direction in response to the forcing effect of curvature and remain proportional to the chosen 'measure' of curvature, i.e. to the small parameter ν. This appears to be a reasonable assumption as long as the behaviour of our system coincides with that of a weakly forced linear oscillator.

In order to derive the ordinary differential problem governing the transverse dependence of (U_1, V_1, H_1, D_1) we further expand τ_s, τ_n, Q_s, Q_n in the form

$$\tau_s = C_0\{1 + \nu[(s_1 U_1 + s_2 D_1)\, e_1 + \text{c.c.}] + O(\nu^2)\}, \tag{21a}$$

$$\tau_n = C_0\{\nu[(V_1 + k_4)\, e_1 + \text{c.c.}] + O(\nu^2)\}, \tag{21b}$$

$$Q_s = \Phi_0\{1 + \nu[(f_1 U_1 + f_2 D_1)\, e_1 + \text{c.c.}] + O(\nu^2)\}, \tag{21c}$$

$$Q_n = \Phi_0\{\nu[(V_1 + k_4 - R(F_0^2 H_{1,n} - D_{1,n}))\, e_1 + \text{c.c.}] + O(\nu^2)\}, \tag{21d}$$

where

$$s_1 = 2\left[1 - \frac{\theta_0}{C_0}(C_{,\theta})_0\right]^{-1}, \quad s_2 = \frac{(C_{,D})_0}{C_0}\left[1 - \frac{\theta_0}{C_0}(C_{,\theta})_0\right]^{-1}, \tag{22a, b}$$

$$f_1 = s_1 \frac{\theta_0}{\Phi_0}(\Phi_{,\theta})_0, \quad f_2 = \frac{(\Phi_{,D})_0}{\Phi_0} + s_2 \frac{\theta_0}{\Phi_0}(\Phi_{,\theta})_0, \quad R = \frac{r}{\beta \theta_0^{\frac{1}{2}}} \tag{22c–e}$$

and subscript 0 denotes unperturbed uniform values of Shields stress, bed-load function and friction coefficient.

Substituting from (20), (21), (22) into the governing differential system (5), (6), (7), (8) and boundary conditions (18), (19), at $O(\nu)$ we find

$$\mathbf{L}\begin{pmatrix} U_1 \\ V_1 \\ H_1 \\ D_1 \end{pmatrix} = \begin{pmatrix} b_1 \\ b_2 \\ b_3 \\ b_4 \end{pmatrix}, \tag{23a–d}$$

$$V_1 = 0 \qquad (n = \pm 1), \tag{23e}$$

$$F_0^2 H_{1,n} - D_{1,n} = b_5 \quad (n = \pm 1), \tag{23f}$$

where

$$\mathbf{L} \equiv \begin{pmatrix} a_{11} & a_{12} & a_{13} & a_{14} \\ a_{21} & a_{22} & a_{23}\dfrac{\mathrm{d}}{\mathrm{d}n} & a_{24} \\ a_{31} & a_{32}\dfrac{\mathrm{d}}{\mathrm{d}n} & a_{33} & a_{34} \\ a_{41} & a_{42}\dfrac{\mathrm{d}}{\mathrm{d}n} & a_{43}\dfrac{\mathrm{d}^2}{\mathrm{d}n^2} & a_{44}\dfrac{\mathrm{d}^2}{\mathrm{d}n^2} + a_{45} \end{pmatrix}, \tag{24}$$

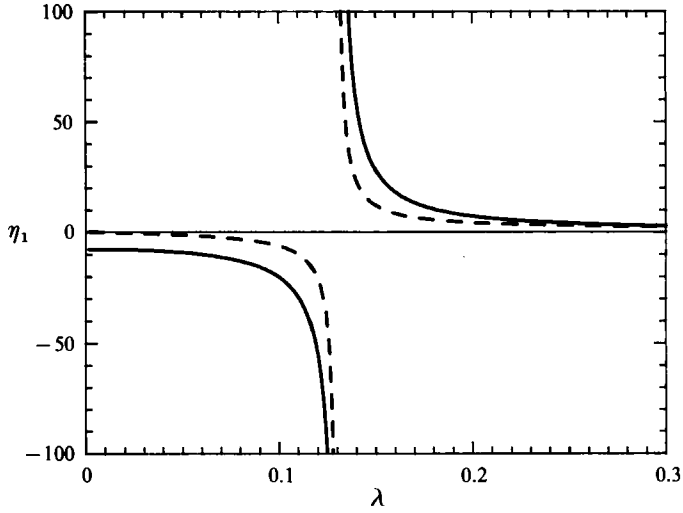

FIGURE 2. Linear response of a meandering channel at resonance: the dimensionless amplitude of bottom elevation η_1 ($= F_0^2 H_1 - D_1$) is plotted versus meander wavenumber λ ($\theta_0 = 0.1$, $d_s = 0.01$, $\beta = 20.$). Solid and dashed curves denote Re (η_1) and Im (η_1) respectively.

with

$$a_{11} = \mathrm{i}\lambda + \beta C_0 s_1, \quad a_{12} = 0, \quad a_{13} = \mathrm{i}\lambda, \quad a_{14} = \beta C_0 (s_2 - 1), \tag{25a–d}$$

$$a_{21} = 0, \quad a_{22} = \mathrm{i}\lambda + \beta C_0, \quad a_{23} = 1, \quad a_{24} = 0, \tag{25e–h}$$

$$a_{31} = \mathrm{i}\lambda, \quad a_{32} = 1, \quad a_{33} = 0, \quad a_{34} = \mathrm{i}\lambda, \tag{25i–l}$$

$$a_{41} = \mathrm{i}\lambda \Phi_0 f_1, \quad a_{42} = \Phi_0, \quad a_{43} = -RF_0^2 \Phi_0, \quad a_{44} = R\Phi_0, \quad a_{45} = \mathrm{i}\lambda \Phi_0 f_2. \tag{25m–q}$$

and

$$b_1 = -n\beta C_0, \quad b_2 = 1 - \mathrm{i}\lambda k_1 - \beta C_0 k_4, \quad b_3 = b_4 = 0, \quad b_5 = k_4/R. \tag{26a–e}$$

The differential problem (23) is readily solved in closed form (see Blondeaux & Seminara 1985). Its solution exhibits the typical features of forced linear oscillators. In particular the amplitude of the response to forcing, i.e. the amplitude of any quantity describing flow or bed topography, exhibits an infinite peak (see figure 2) for values of the relevant parameters (the width-to-depth ratio of the undisturbed channel β and the meander wavenumber λ) such that a natural response of the channel is excited. Figures 3 and 4 respectively show the resonant values λ_R and β_R as functions of θ_0 and d_s both for the plane case and for the dune case.

Blondeaux & Seminara (1985) pointed out that the natural response of the channel excited at resonance coincides with a marginally stable and non-migrating alternating bar (i.e. temporally neither amplifying nor decaying). The latter also coincides with the marginally stable spatially growing bar perturbation first investigated by Olesen (1983). This is readily shown. In fact the linear stability of the basic uniform flow to spatially growing disturbances can be investigated by setting

$$(U, V, H, D) = (1, O, H_0, 1) + [(U_1, V_1, H_1, D_1) \exp(\mathrm{i}\lambda s) + \text{c.c.}] \tag{27}$$

and assuming the amplitude (U_1, V_1, H_1, D_1) to be infinitesimal with λ a complex wavenumber such that $(-\mathrm{Im}(\lambda))$ is the spatial growth rate of perturbations. The governing differential problem for (U_1, V_1, H_1, D_1) is then found by substituting from (27) into the linearized form of (5), (6), (7), (8), (18), (19) with ν set equal to zero and λ assumed to be complex. One finds a differential system identical with the homogeneous part of (23), λ being now complex. Such a system poses an eigenvalue

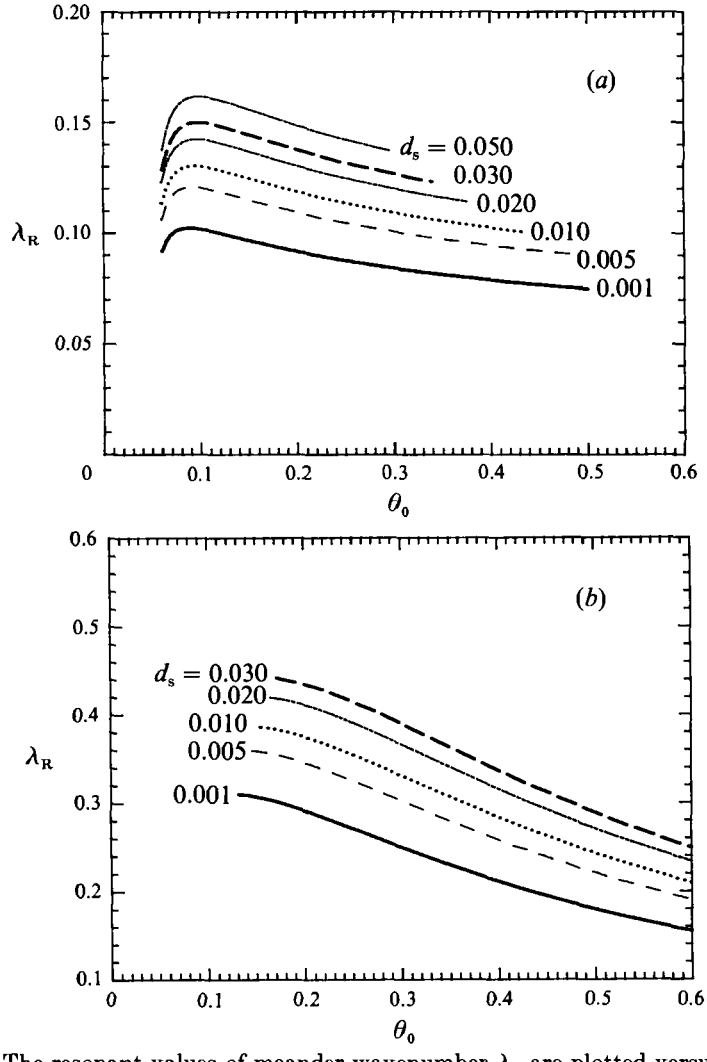

FIGURE 3. The resonant values of meander wavenumber λ_R are plotted versus Shields stress θ_0 for given values of dimensionless grain roughness d_s: (*a*) plane bed; (*b*) dune-covered bed.

problem for λ which can be shown (see Struiksma *et al.* 1985; Seminara 1989) to have four complex solutions. In general two of them are purely imaginary and correspond to exponentially damped or growing perturbations, while the remaining two complex solutions describe damped (or growing) spatial oscillations. However, a restricted range of β may exist where all the solutions are purely imaginary. Figure 5(*a*, *b*) show typical plots of Re (λ) and Im (λ) as functions of β for given values of θ_0 and d_s in the plane and dune case respectively. The resonant values λ_R and β_R are defined by the condition

$$\mathrm{Im}\,(\lambda) = 0, \tag{28}$$

i.e. by the values of Re (λ) and β corresponding to the intersections of the dashed lines of figure 5(*a*, *b*) with the vertical axis. The eigenfunctions belonging to such eigenvalues are readily found to be of the form

$$(U_1^R, V_1^R, H_1^R, D_1^R) = A(S_1, C_1, S_1, S_1) \tag{29}$$

with $$S_m = \sin(\tfrac{1}{2}\pi mn), \quad C_m = \cos(\tfrac{1}{2}\pi mn) \quad (m = 1, 2, 3, \ldots) \tag{30a, b}$$

and A an arbitrary infinitesimal constant.

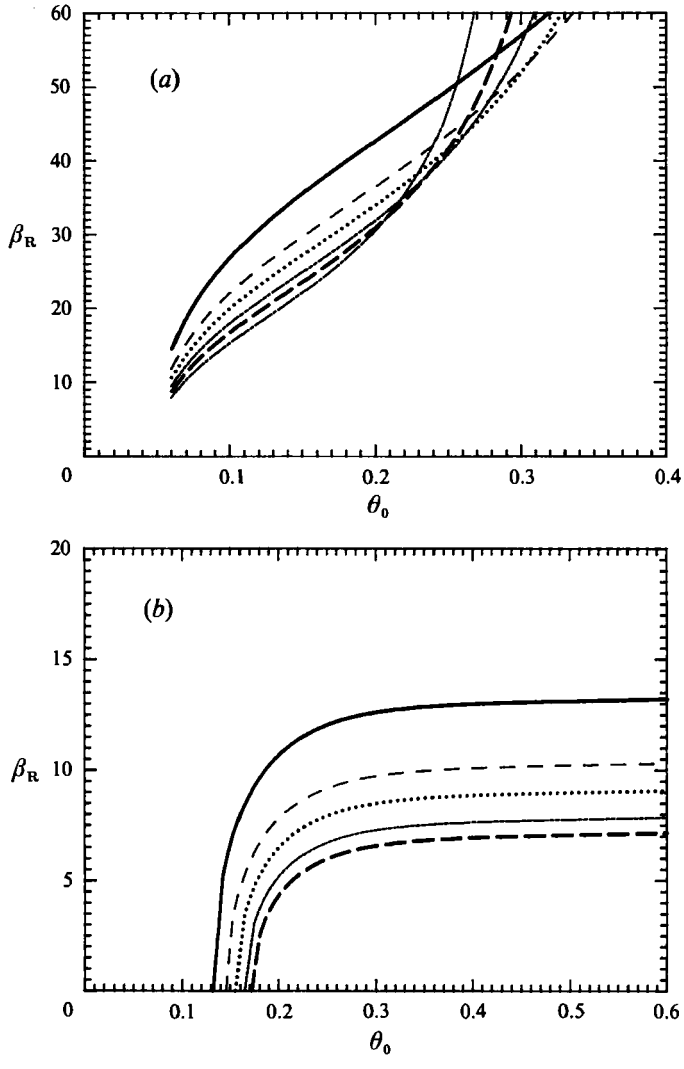

FIGURE 4. The resonant values of the width ratio of the channel β_R are plotted versus Shields stress θ_0 for given values of dimensionless grain roughness d_s (d_s ranges as in figure 3): (*a*) plane bed; (*b*) dune-covered bed.

It is worth pointing out that the eigensolution described above is only the first of an infinite sequence of 'modes', each corresponding to a different value of m. Higher-order modes are such that their resonant conditions correspond to increasingly higher values of β and λ according to the following relationships:

$$\beta_R^{(m)} = m\beta_R, \quad \lambda_R^{(m)} = m\lambda_R. \tag{31a, b}$$

In the present investigation we are only concerned with the first spatially growing mode, corresponding to $m = 1$. The experiments of Struiksma *et al.* (1985) and Struiksma & Crosato (1989) clearly show that the above perturbations do arise in response to some finite perturbation of the initial conditions for flow and bed topography.

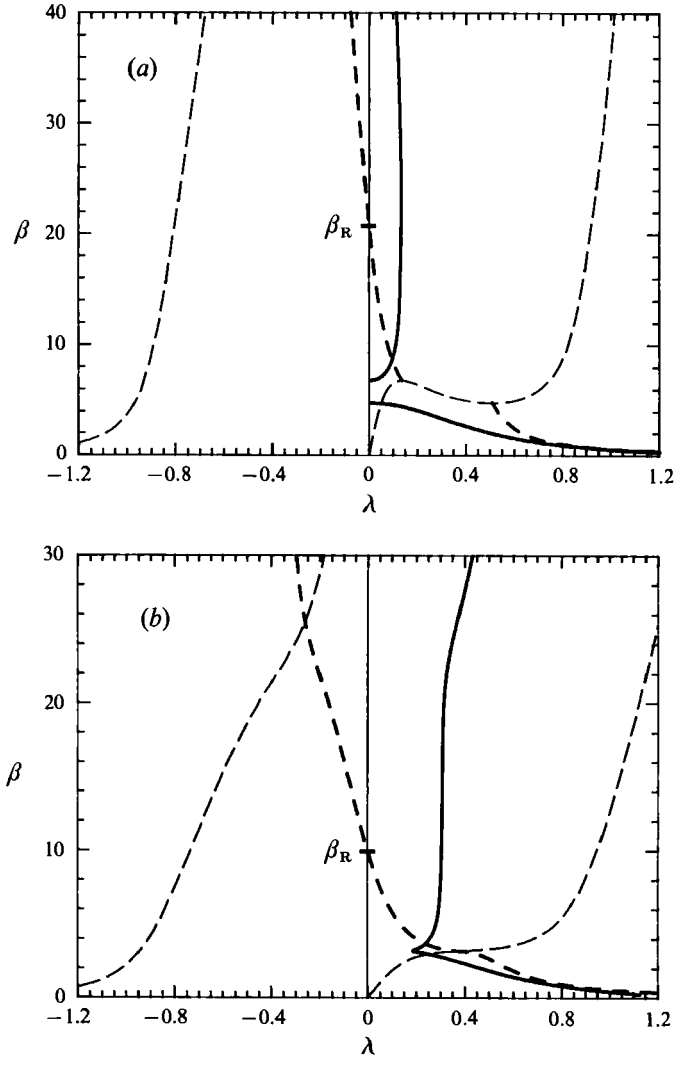

FIGURE 5. The complex wavenumber λ of spatially growing bars as a function of the width ratio β. Solid and dashed curves denote Re (λ) and Im (λ) respectively: (*a*) $\theta_0 = 0.1$, $d_s = 0.01$, plane bed; (*b*) $\theta_0 = 0.3$, $d_s = 0.005$, dune-covered bed.

However, both the linear theory of meanders and the linear theory of spatially growing bars are restricted by the severe limitation of linearity of perturbations. The latter implies an unbounded response of meanders at resonance and an indefinite exponential growth of spatially growing bars for $\beta > \beta_R$. In the next sections we show that nonlinearity prevents both of the above effects through mechanisms which are strongly interrelated.

4. Weakly nonlinear evolution of spatially growing bars in straight channels

The theory of weakly nonlinear development of spatially growing steady bars in straight cohesionless channels is strongly related to the theory of temporally growing migrating bars proposed by Colombini *et al.* (1987) (hereinafter referred to as CST).

Hence we set $\nu \equiv 0$ in (5), (6), (7), (8), (18), (19) and seek a finite-amplitude solution restricting our attention to the weakly nonlinear regime defined by the conditions

$$\beta = \beta_{\mathrm{R}}(1+\epsilon), \quad \mathrm{Re}\,(\lambda) = \lambda_{\mathrm{R}} \tag{32a, b}$$

with $\epsilon \ll 1$. Physically (32) describe an experiment where in a uniform straight channel flow with cohesionless bottom, characterized by width aspect ratio β slightly perturbed with respect to the threshold value β_{R} for spatial growth of perturbations, a steady perturbation is imposed in the initial cross-section and is allowed to grow spatially. We now investigate whether the initial perturbation asymptotically reaches an equilibrium amplitude.

The weakly nonlinear theory of CST is readily modified to describe spatial rather than temporal development. Herein we do not wish to repeat CST's analysis but merely emphasize the modifications required to allow for spatial rather than temporal growth and refer the reader to CST for details.

Let us introduce a spatial 'slow variable' ζ such that

$$\zeta = \epsilon s; \tag{33}$$

hence we can make the following substitution

$$\frac{\partial}{\partial s} \rightarrow \frac{\partial}{\partial s} + \epsilon \frac{\partial}{\partial \zeta}. \tag{34}$$

Following CST we can analyse the cascade process induced by weakly nonlinear interactions of the fundamental 'spatial' perturbation with itself and with the basic flow. Hence we are led to derive an expansion for the weakly nonlinear solution in powers of $\epsilon^{\frac{1}{2}}$ in the form

$$\begin{aligned}
(U, D, H, V) = {} & (1, 1, H_0, 0) && \text{(basic flow)} \\
& + \epsilon^{\frac{1}{2}}\{A(\zeta)\, e_1^{\mathrm{R}}\, [S_1(u_1^{\mathrm{R}}, d_1^{\mathrm{R}}, h_1^{\mathrm{R}}), C_1 v_1^{\mathrm{R}}] + \text{c.c.}\} && \text{(fundamental)} \\
& + \epsilon\{A^2 e_2^{\mathrm{R}}\, [(C_2(u_{22}^{\mathrm{R}}, d_{22}^{\mathrm{R}}, h_{22}^{\mathrm{R}}), S_2 v_{22}^{\mathrm{R}}) \\
& + (u_{02}^{\mathrm{R}}, d_{02}^{\mathrm{R}}, h_{02}^{\mathrm{R}}, v_{02}^{\mathrm{R}})] + \text{c.c.} \\
& + |A|^2 [(C_2(u_{20}^{\mathrm{R}}, d_{20}^{\mathrm{R}}, h_{20}^{\mathrm{R}}), S_2 v_{20}^{\mathrm{R}}) + (u_{00}^{\mathrm{R}}, d_{00}^{\mathrm{R}}, h_{00}^{\mathrm{R}}, v_{00}^{\mathrm{R}})]\} && \text{(second harmonics)} \\
& + \epsilon^{\frac{3}{2}}\{e_1^{\mathrm{R}}\, [S_1(u_{11}^{\mathrm{R}}(\zeta), d_{11}^{\mathrm{R}}(\zeta), h_{11}^{\mathrm{R}}(\zeta)), C_1 v_{11}^{\mathrm{R}}(\zeta)] + \text{c.c.}\} \\
& + O(\epsilon^{\frac{3}{2}}) && \text{(higher harmonics)} \qquad (35a)
\end{aligned}$$

where

$$e_m^{\mathrm{R}} = \exp[m(\mathrm{i}\lambda_{\mathrm{R}} s)] \quad (m = 1, 2, \ldots). \tag{35b}$$

The reader aware of CST's work will recognize that the structure of (35) is identical with that developed in CST to analyse temporally growing bars, but for two fundamental differences:

(i) the solution is centred around the critical conditions for spatial (rather than temporal) growth, namely

$$\mathrm{Re}\,(\lambda) = \lambda_{\mathrm{R}}, \quad \beta = \beta_{\mathrm{R}}, \quad \omega = 0, \tag{36a–c}$$

with ω denoting the angular frequency of perturbations;

(ii) the complex amplitude A is a slowly varying function of space rather than time.

An expansion similar to (35) can be set up for $(\tau_s, \tau_n, Q_s, Q_n)$ (see (29), (14), (33) and (48) of CST). The latter, substituted in (5)–(8) along with (32), (33), (34), (35) and with the condition of vanishing ν, leads to a cascade of linear algebraic systems which, up to order ϵ, are identical with those found in CST except for the parameters $(\lambda_{\mathrm{R}}, \beta_{\mathrm{R}}, 0)$ replacing $(\lambda_{\mathrm{c}}, \beta_{\mathrm{c}}, \omega_{\mathrm{c}})$. Hence we simply recall the main results for completeness.

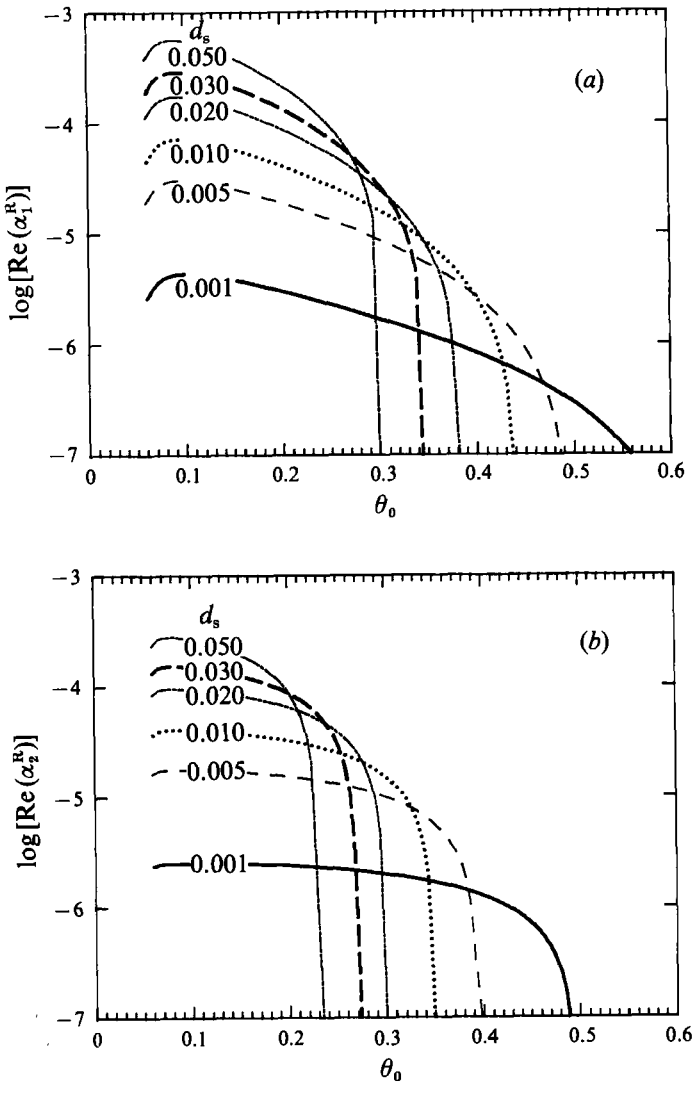

FIGURE 6. The real parts of the coefficients α_1^R and α_2^R of the amplitude equation for steady bars are given as functions of Shields stress θ_0 and grain roughness parameter d_s (plane bed): (*a*) $\mathrm{Re}(\alpha_1^R)$; (*b*) $\mathrm{Re}(\alpha_2^R)$.

$O(\epsilon^{\frac{1}{2}})$

The linear algebraic system for $(u_1^R, v_1^R, h_1^R, d_1^R)$ reads

$$L_{11}^R \begin{pmatrix} u_1^R \\ v_1^R \\ h_1^R \\ d_1^R \end{pmatrix} = (a_{i1}^R u_1^R + a_{i2}^R v_1^R + a_{i3}^R h_1^R + a_{i4}^R d_1^R) = 0 \quad (i = 1,2,3,4) \qquad (37a\text{–}d)$$

where $L_{pq}^R (p = 1,2,\ldots; q = 1,2,\ldots)$ is the linear algebraic operator obtained from the linear differential operator $\mathbf{L}$ defined in (24) replacing $[\mathrm{Re}(\lambda), \mathrm{Im}(\lambda), \beta, \mathrm{d}/\mathrm{d}n, \mathrm{d}^2/\mathrm{d}n^2]$ by $[q\lambda_R, 0, \beta_R, \frac{1}{2}p\pi(-1)^p, -(\frac{1}{2}p\pi)^2]$ everywhere but in a_{23} where $(\mathrm{d}/\mathrm{d}n)$ is replaced by $[(-1)^{p-1}p\pi]$. Notice that (λ_R, β_R) are eigenvalues of (37) since they satisfy the dispersion relationship associated with (37).

$O(\epsilon)$

The algebraic systems governing the coefficients of second harmonics are non-homogeneous and may be written in the general form

$$L^{\mathrm{R}}_{pq}\begin{pmatrix} u^{\mathrm{R}}_{pq} \\ v^{\mathrm{R}}_{pq} \\ h^{\mathrm{R}}_{pq} \\ d^{\mathrm{R}}_{pq} \end{pmatrix} = \begin{pmatrix} b^{pq}_1 \\ b^{pq}_2 \\ b^{pq}_3 \\ b^{pq}_4 \end{pmatrix}, \tag{38a–d}$$

where the non-homogeneous terms $b^{pq}_1, b^{pq}_2, b^{pq}_3, b^{pq}_4$ are obtained from (37), (38), (39), (40) of CST.

$O(\epsilon^{\frac{3}{2}})$

Finally the linear system for the coefficients of the fundamental reproduced at third order is readily found to have the form

$$L^{\mathrm{R}}_{11}\begin{pmatrix} u^{\mathrm{R}}_{11} \\ v^{\mathrm{R}}_{11} \\ h^{\mathrm{R}}_{11} \\ d^{\mathrm{R}}_{11} \end{pmatrix} = \begin{pmatrix} p^{\mathrm{R}}_1 A|A|^2 + p^{\mathrm{R}}_2 A + p^{\mathrm{R}}_9 \dfrac{\mathrm{d}A}{\mathrm{d}\zeta} \\ p^{\mathrm{R}}_3 A|A|^2 + p^{\mathrm{R}}_4 A + p^{\mathrm{R}}_{10} \dfrac{\mathrm{d}A}{\mathrm{d}\zeta} \\ p^{\mathrm{R}}_5 A|A|^2 + p^{\mathrm{R}}_6 A + p^{\mathrm{R}}_{11} \dfrac{\mathrm{d}A}{\mathrm{d}\zeta} \\ p^{\mathrm{R}}_7 A|A|^2 + p^{\mathrm{R}}_8 A + p^{\mathrm{R}}_{12} \dfrac{\mathrm{d}A}{\mathrm{d}\zeta} \end{pmatrix}, \tag{39a–d}$$

where the quantities p^{R}_{1-8} coincide with the corresponding quantities of (50) of CST, with $(\lambda_{\mathrm{c}}, \beta_{\mathrm{c}}, \omega_{\mathrm{c}})$ replaced by $(\lambda_{\mathrm{R}}, \beta_{\mathrm{R}}, 0)$, while p^{R}_9, p^{R}_{10}, p^{R}_{11}, p^{R}_{12} are

$$p^{\mathrm{R}}_9 = -u^{\mathrm{R}}_1 - h^{\mathrm{R}}_1, \quad p^{\mathrm{R}}_{10} = -v^{\mathrm{R}}_1, \quad p^{\mathrm{R}}_{11} = -u^{\mathrm{R}}_1 - d^{\mathrm{R}}_1, \quad p^{\mathrm{R}}_{12} = -\Phi_0(f_1 u^{\mathrm{R}}_1 + f_2 d^{\mathrm{R}}_1). \tag{40a–d}$$

For the system (39) a solvability condition has to be satisfied because its homogeneous part admits a non-trivial solution. Solvability requires that the following condition be satisfied:

$$\begin{vmatrix} a^{\mathrm{R}}_{11} & a^{\mathrm{R}}_{12} & a^{\mathrm{R}}_{13} & A|A|^2 p^{\mathrm{R}}_1 + p^{\mathrm{R}}_2 A + p^{\mathrm{R}}_9 \dfrac{\mathrm{d}A}{\mathrm{d}\zeta} \\ a^{\mathrm{R}}_{21} & a^{\mathrm{R}}_{22} & a^{\mathrm{R}}_{23} & A|A|^2 p^{\mathrm{R}}_3 + p^{\mathrm{R}}_4 A + p^{\mathrm{R}}_{10} \dfrac{\mathrm{d}A}{\mathrm{d}\zeta} \\ a^{\mathrm{R}}_{31} & a^{\mathrm{R}}_{32} & a^{\mathrm{R}}_{33} & A|A|^2 p^{\mathrm{R}}_5 + p^{\mathrm{R}}_6 A + p^{\mathrm{R}}_{11} \dfrac{\mathrm{d}A}{\mathrm{d}\zeta} \\ a^{\mathrm{R}}_{41} & a^{\mathrm{R}}_{42} & a^{\mathrm{R}}_{43} & A|A|^2 p^{\mathrm{R}}_7 + p^{\mathrm{R}}_8 A + p^{\mathrm{R}}_{12} \dfrac{\mathrm{d}A}{\mathrm{d}\zeta} \end{vmatrix} = 0. \tag{41}$$

From (41) the following nonlinear amplitude equation is readily derived:

$$\alpha^{\mathrm{R}}_0 \frac{\mathrm{d}A}{\mathrm{d}\zeta} + \alpha^{\mathrm{R}}_1 A + \alpha^{\mathrm{R}}_2 A|A|^2 = 0, \tag{42}$$

where α^{R}_1 and α^{R}_2 are obtained from the corresponding complex coefficients α_1 and α_2

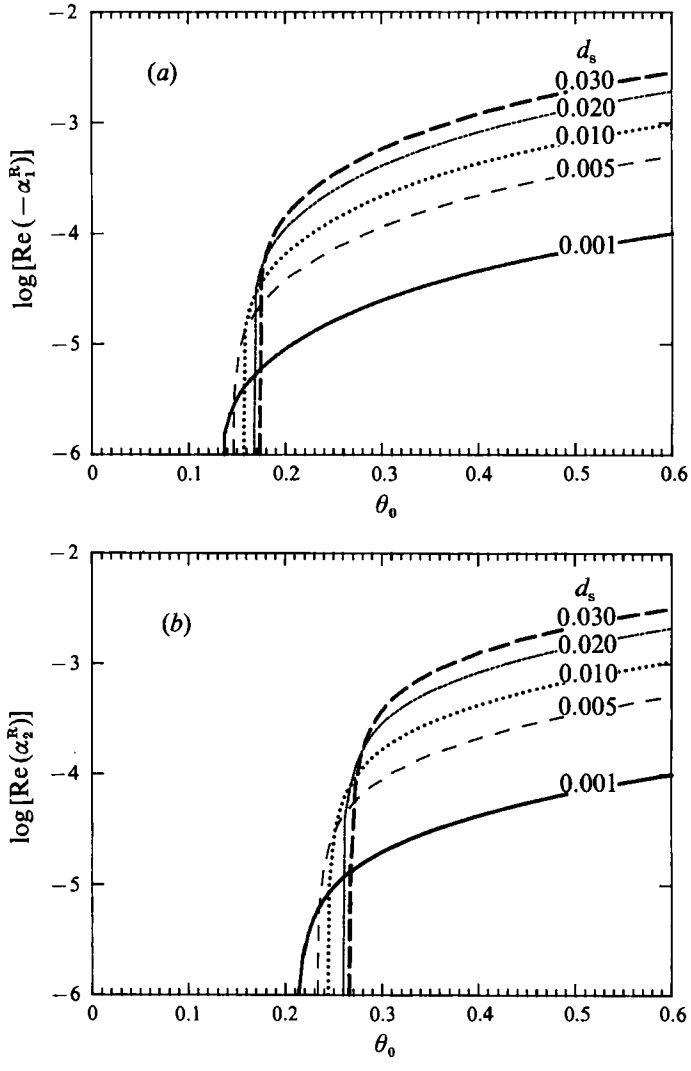

FIGURE 7. The real parts of the coefficients α_1^R and α_2^R of the amplitude equation for steady bars are given as function of Shields stress θ_0 and grain roughness parameter d_s (dune-covered bed): (*a*) $\mathrm{Re}(\alpha_1^R)$; (*b*) $\mathrm{Re}(\alpha_2^R)$.

of the amplitude equation (52) of CST for temporally growing bars (evaluated at resonance) and

$$\alpha_0^R = \frac{p_{12}^R D_{123}^R - p_9^R D_{234}^R + p_{10}^R D_{134}^R - p_{11}^R D_{124}^R}{p_9 D_{123}}. \tag{43}$$

In (43) D_{ijk}^R denotes the determinant

$$D_{ijk}^R \equiv \begin{vmatrix} a_{i1}^R & a_{i2}^R & a_{i3}^R \\ a_{j1}^R & a_{j2}^R & a_{j3}^R \\ a_{k1}^R & a_{k2}^R & a_{k3}^R \end{vmatrix}. \tag{44}$$

D_{123} has the form (44) with a_{lk}^R replaced by the coefficients a_{lk} of CST, and p_9 is the coefficient appearing in (50) of CST.

The amplitude equation (42) is of Landau–Stuart type. Hence provided

$$sgn\,[Re\,(\alpha_2^{\mathrm{R}})] \neq \mathrm{sgn}\,[\mathrm{Re}\,(\alpha_1^{\mathrm{R}})]$$

it exhibits a supercritical equilibrium solution:

$$|A_{\mathrm{e}}| = [-\mathrm{Re}\,(\alpha_1^{\mathrm{R}})/\mathrm{Re}\,(\alpha_2^{\mathrm{R}})]^{\frac{1}{2}}. \tag{45}$$

In figures 6(*a*, *b*) and 7(*a*, *b*) we plot $\mathrm{Re}\,(\alpha_1^{\mathrm{R}})$ and $\mathrm{Re}\,(\alpha_2^{\mathrm{R}})$ as functions of θ_0 and d_{s} for the plane and dune cases respectively. These plots show the supercritical character of the bifurcation within a wide range of values of Shields and grain roughness parameters, which confirms that under supercritical conditions the initial perturbation does develop asymptotically in space into an equilibrium periodic configuration consisting of steady bars.

5. Weakly nonlinear theory of near-resonant meanders

Let us now investigate flow and bed topography in weakly meandering channels characterized by wavenumber λ and undisturbed width-to-depth ratio β falling within a neighbourhood of the resonant values, λ_{R} and β_{R} respectively, for given values of the unperturbed Shields stress θ_0 and grain roughness d_{s}. We look for a solution of the nonlinear problem (5)–(8) such that the singular resonant behaviour occurring at the linear level be suppressed.

The main questions to which we need preliminary answers are:

(i) what is the order of magnitude of the amplitude of the solution in terms of the small parameter ν such that suppression of the singularity may be achieved?

(ii) what is the width of the 'resonant range' to be investigated?

We are mainly concerned here with steady-state solutions of the problem. However, it will prove useful in the following to know the transient behaviour of the channel response. A preliminary prediction of the latter behaviour requires an answer to a third question:

(iii) what is the timescale of the transient?

In order to answer the above questions we follow a classical argument employed in analysing weakly nonlinear resonant oscillations. Let us assume the fundamental component of the perturbation to be of order ν^x with x a real exponent to be determined. Moreover, at lowest order, exactly at resonance, the solution must coincide with the 'natural' solution of the homogeneous linear problem describing marginally stable non-migrating and non-amplifying free bars. Hence at lowest order we can write

$$(U, H, D, V) = \nu^x\{A[(u_1^{\mathrm{R}}, h_1^{\mathrm{R}}, d_1^{\mathrm{R}})\,S_1, v_1^{\mathrm{R}}\,C_1]\,e_1^{\mathrm{R}} + \mathrm{c.c.}\}, \tag{46}$$

with A a complex amplitude function to be determined.

Nonlinear interactions involving the fundamental and the basic uniform flow produce at second order, $O(\nu^{2x})$, second harmonics, both longitudinal and transverse. At third order, $O(\nu^{3x})$, the fundamental is reproduced giving rise to secular terms. Hence, provided the condition

$$3x = 1 \tag{47}$$

is satisfied, the reproduction of the fundamental occurs at the same order, $O(\nu)$, as the forcing effect of curvature and the requirement of suppression of secular terms also leads to suppressing the singular behaviour of the solution predicted by the linear theory.

Similarly, for variations of β and λ in a neighbourhood of β_R and λ_R respectively to be felt at order ν, their order must be $\nu^{\frac{2}{3}}$.

Finally a similar argument suggests that the time variable appropriate to describe the transient evolution of the amplitude function A is the 'slow' variable T defined as $(\nu^{\frac{2}{3}}t)$.

Hence we expand the solution in the following form

$$\beta = \beta_R(1+\nu^{\frac{2}{3}}\beta_1), \quad \lambda = \lambda_R + \nu^{\frac{2}{3}}\lambda_1, \quad T = \nu^{\frac{2}{3}}t, \tag{48a–c}$$

$$\begin{aligned}(U,H,D) = {} & (1,H_0,1) + \nu^{\frac{1}{3}}[AS_1\, e_1^R(u_1^R,h_1^R,d_1^R) + \text{c.c.}] \\ & + \nu^{\frac{2}{3}}\{A^2 e_2^R\,[C_2(u_{22}^R,h_{22}^R,d_{22}^R) + (u_{02}^R,h_{02}^R,d_{02}^R)] + \text{c.c.} \\ & + |A|^2[C_2(u_{20}^R,h_{20}^R,d_{20}^R) + (u_{00}^R,h_{00}^R,d_{00}^R)]\} \\ & + \nu\{e_1^R\,[U_{11}(n),H_{11}(n),D_{11}(n)] + \text{c.c.}\} + O(\nu^{\frac{4}{3}},\nu e_3^R),\end{aligned} \tag{49}$$

$$\begin{aligned}V = {} & \nu^{\frac{1}{3}}(AC_1\, e_1^R v_1^R) + \nu^{\frac{2}{3}}[(A^2 e_2^R v_{22}^R S_2 + \text{c.c.}) + |A|^2 v_{20}^R S_2] \\ & + \nu[e_1^R V_{11}(n) + \text{c.c.}] + O(\nu^{\frac{4}{3}},\nu e_3^R),\end{aligned} \tag{50}$$

where β_1 and λ_1 are $O(1)$ constants.

The expansions (49) and (50) clearly show that the fundamental component of the perturbation and the second harmonics have a structure identical with that of the finite-amplitude spatial bars investigated in the previous section. The characteristic feature of the present solution is that the amplitude of the perturbation is not controlled by a bifurcation process from the basic uniform solution, as in the case of finite-amplitude spatial bars, but rather by the forcing effect of curvature and by nonlinearity. As a result the amplitude equation governing the dependence of the amplitude function A on the relevant parameters will be seen to exhibit some non-homogeneous contribution associated with channel curvature.

On substituting from (48), (49) and (50) into the governing equations and equating terms of order $\nu^{\frac{1}{3}}$ we obviously recover the unforced linear algebraic problem (37). Similarly equating terms of order $\nu^{\frac{2}{3}}$ we recover problems for the harmonics 22, 20, 02 and 00 which are still unaffected by curvature, hence coincide with the linear algebraic systems (38) discussed in the previous sections.

At third order, $O(\nu)$, the linear algebraic system governing the fundamental reproduced by nonlinear interactions includes non-homogeneous terms associated with curvature. We find

$$\mathbf{L}^R\begin{pmatrix}U_{11}\\V_{11}\\H_{11}\\D_{11}\end{pmatrix} = \begin{pmatrix}S_1[p_1^R\, A|A|^2 + \hat{p}_2^R A] + b_1^R \\ C_1[p_3^R A|A|^2 + \hat{p}_4^R A] + b_2^R \\ S_1[p_5^R A|A|^2 + \hat{p}_6^R A] + b_3^R \\ S_1\left[p_7^R A|A|^2 + \hat{p}_8^R A + p_{13}^R \dfrac{dA}{dT}\right] + b_4^R\end{pmatrix}, \tag{51a–d}$$

$$V_{11} = 0 \qquad (n = \pm 1),$$

$$(F_0^2 H_{11} - D_{11})_{,n} = b_5^R \quad (n = \pm 1), \tag{51e,f}$$

where $\mathbf{L}^R$ is the linear differential operator $\mathbf{L}$ defined in (24), b_{1-5}^R are the quantities given by (26a–e), all evaluated at resonant conditions ($\lambda = \lambda_R, \beta = \beta_R$) and

$$\hat{p}_2^R = \beta_1 p_2^R + i\lambda_1 p_9^R, \quad \hat{p}_4^R = \beta_1 p_4^R + i\lambda_1 p_{10}^R,$$

$$\hat{p}_6^R = \beta_1 p_6^R + i\lambda_1 p_{11}^R, \quad \hat{p}_8^R = \beta_1 p_8^R + i\lambda_1 p_{12}^R. \tag{52a–d}$$

Furthermore p_{13}^R is

$$p_{13}^R = d_1^R - F_0^2 h_1^R. \tag{53}$$

Since the homogeneous part of the differential problem (51) admits a non-trivial solution we require that a solvability condition must be satisfied (see Coddington & Levinson 1955, p. 294). A convenient procedure to derive the solvability condition is to transform (51) into a single-order ordinary differential equation for V_{11} with suitable boundary conditions. By constructing an appropriate set of adjoint complementary boundary forms and imposing the Fredholm alternative we find the following amplitude equation:

$$\frac{\mathrm{d}A}{\mathrm{d}T}+\hat{\alpha}_1^{\mathrm{R}}A+\alpha_2^{\mathrm{R}}A\,|A|^2+\alpha_3^{\mathrm{R}}=0, \quad \hat{\alpha}_1=\beta_1\alpha_1^{\mathrm{R}}+\mathrm{i}\lambda_1\alpha_0^{\mathrm{R}}, \tag{54a, b}$$

where α_0^{R}, α_1^{R}, α_2^{R} are identical with the complex coefficients of the amplitude equation (42) describing the finite-amplitude development of spatially growing bars, and $\alpha_3^{\mathrm{R}}$is the non-homogeneous terms associated with the forcing effect of curvature.

We point out that (54a) represents the fundamental result of the present theory. Its solution gives the dependence of the complex amplitude A on the parameters of the problem and through the expansions (48), (49), (50) completely determines the solution for the flow and bottom topography in weakly meandering channels up to third order.

6. Solutions of the amplitude equation and their stability

Equation (54) admits steady-state solutions A_{e} which can be obtained in the following closed form

$$A_{\mathrm{e}}=-\frac{\alpha_3^{\mathrm{R}}}{\hat{\alpha}_1^{\mathrm{R}}+\alpha_2^{\mathrm{R}}|A_{\mathrm{e}}|^2}, \tag{55}$$

where $|A_{\mathrm{e}}|^2$ is a solution of the following cubic algebraic equation derived from (54a) and (55):

$$(|A_{\mathrm{e}}|^2)^3+\frac{\hat{\alpha}_1^{\mathrm{R}}\bar{\alpha}_2^{\mathrm{R}}+\mathrm{c.c.}}{|\alpha_2^{\mathrm{R}}|^2}(|A_{\mathrm{e}}|^2)^2+\frac{|\hat{\alpha}_1^{\mathrm{R}}|^2}{|\alpha_2^{\mathrm{R}}|^2}(|A_{\mathrm{e}}|^2)-\frac{|\alpha_3^{\mathrm{R}}|^2}{|\alpha_2^{\mathrm{R}}|^2}=0 \tag{56}$$

(herein an overbar denotes the complex conjugate).

In general (56) exhibits one real and two complex-conjugate solutions. Under these conditions, the complex solutions being meaningless, the response of the channel is unique (see figure 8a, b). However, as shown in figure 8(a), ranges of λ_1 exists, for given θ_0 and d_{s}, in which the three solutions of (56) are all real. Hence the response of the channel may not be unique. This feature of the present results is hardly surprising as it characterizes the nonlinear behaviour of resonant oscillators (see, for instance, Thompson & Stewart 1986, p. 72). However, this finding poses the problem of ascertaining which of the three real solutions is appropriate for a given set of initial conditions. In order to answer this question we investigate the linear stability of the above three solutions. Let us then set

$$A=A_{\mathrm{e}}+a \tag{57}$$

and assume a to be infinitesimally small. On substituting from (57) into (54a) and linearizing we find the following linear ordinary differential equation for $a(T)$:

$$\frac{\mathrm{d}a}{\mathrm{d}T}=\gamma_1 a+\gamma_2\bar{a}, \tag{58}$$

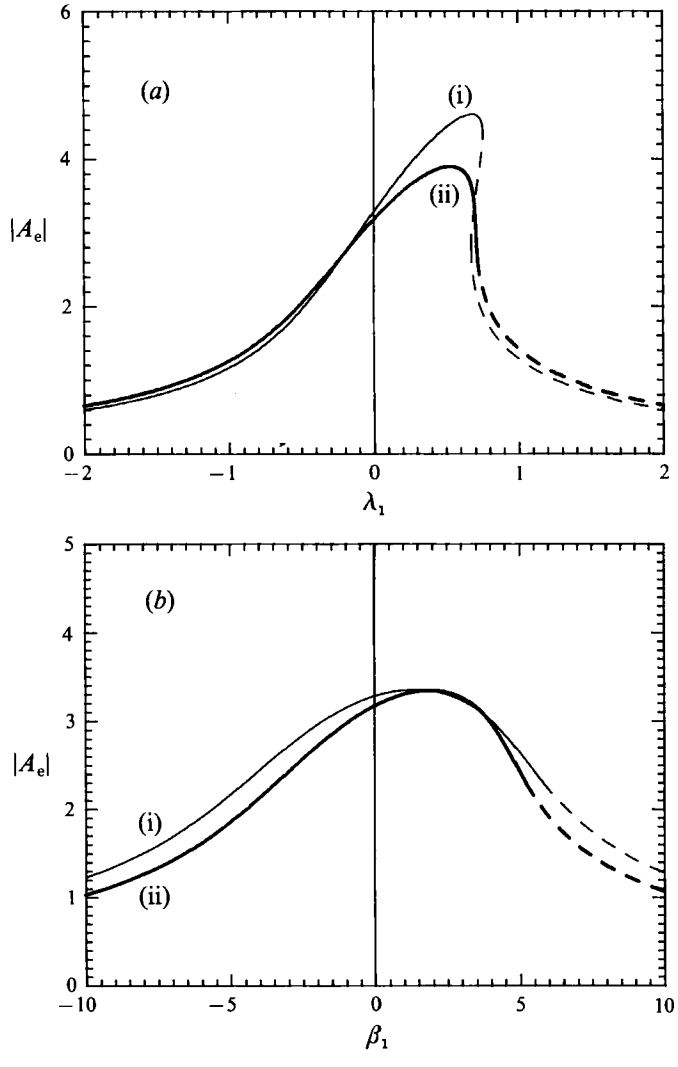

FIGURE 8. The weakly nonlinear steady-state solution for the amplitude function of near-resonant meanders is plotted versus the perturbations (*a*) of meander wavenumber λ_1 and (*b*) of channel width ratio β_1 with respect to the resonant values, for different values of Shields stress θ_0 and grain roughness d_s: (i) $\theta_0 = 0.1$, $d_s = 0.01$; (ii) $\theta_0 = 0.08$, $d_s = 0.05$. Solid and dashed lines denote stable and unstable solutions respectively.

where the complex coefficients γ_1 and γ_2 have the form

$$\gamma_1 = -\hat{\alpha}_1^{\mathrm{R}} - 2\alpha_2^{\mathrm{R}} |A_e|^2, \quad \gamma_2 = -\alpha_2^{\mathrm{R}} A_e^2. \tag{59a, b}$$

From (58) simple algebraic manipulations lead to the following ordinary differential equation:

$$\frac{\mathrm{d}^2 a}{\mathrm{d}T^2} - (\gamma_1 + \bar{\gamma}_1)\frac{\mathrm{d}a}{\mathrm{d}T} + (\gamma_1 \bar{\gamma}_1 - \gamma_2 \bar{\gamma}_2)\, a = 0. \tag{60}$$

Let us set

$$r_1 = -(\gamma_1 + \bar{\gamma}_1), \quad r_2 = \gamma_1 \bar{\gamma}_1 - \gamma_2 \bar{\gamma}_2 \tag{61a, b}$$

$$\mu_1 = \tfrac{1}{2}[-r_1 + (r_1^2 - 4r_2)^{\frac{1}{2}}], \quad \mu_2 = \tfrac{1}{2}[-r_1 - (r_1^2 - 4r_2)^{\frac{1}{2}}]. \tag{62a, b}$$

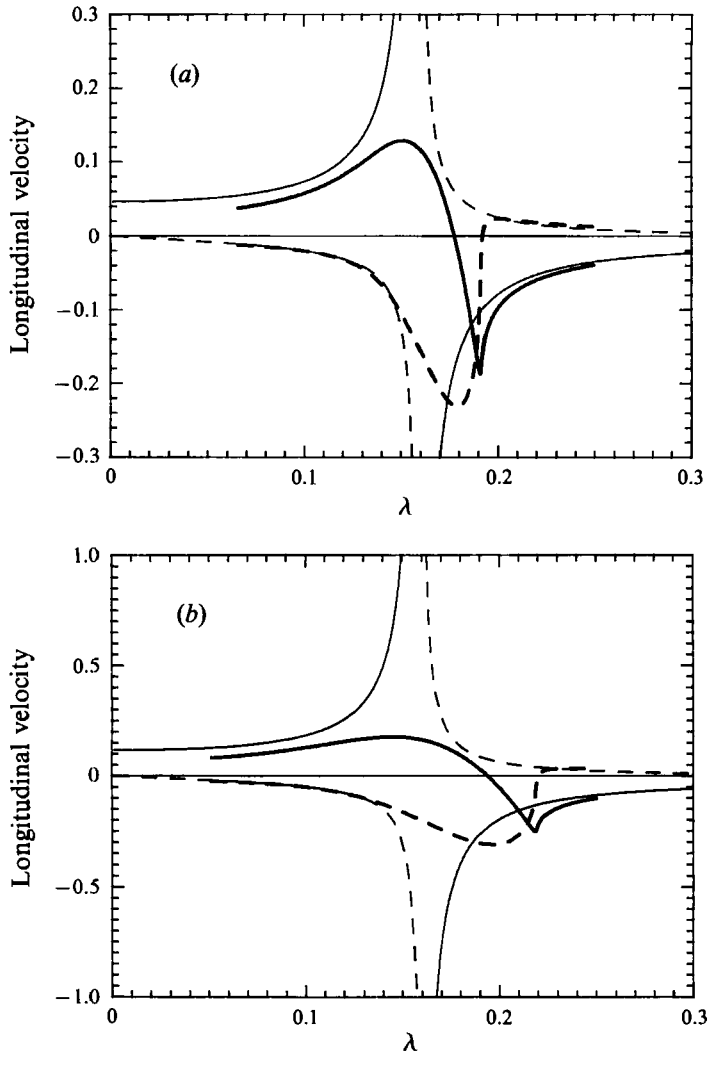

FIGURE 9. The linear solution and the fundamental component of the weakly nonlinear solution for the perturbation of the longitudinal velocity at the outer wall are plotted versus meander wavenumber λ for different values of the curvature ratio ν ($\theta_0 = 0.08$, $d_s = 0.05$, $\beta = 12$). Thin curves: linear theory $[\nu U_1]_{n-1}$; thick curves: nonlinear theory $[\nu^{\frac{1}{2}} A u_1^R]$. Solid and dashed curves denote real and imaginary parts respectively. (*a*) $\nu = 0.01$; (*b*) $\nu = 0.025$.

It follows that the stability of the steady-state solutions is governed by the sign of the real part of μ_1 and μ_2. Since both r_1 and r_2 are real quantities, it follows that solutions are unstable if r_2 is negative or if r_2 is positive with r_1 negative, stable otherwise. Calculations reveal that the upper branch of the solution (see figure 8) is invariably stable while the lower branch and the loop joining the upper branch to the lower branch are invariably unstable.

The latter finding suggests that the fully nonlinear equation (54*a*) has to be solved in order to ascertain the structure of the possibly unsteady solutions bifurcating from the unstable steady solutions. We have solved (54*a*) numerically by means of a Runge–Kutta scheme of fourth order. The numerical solution shows that the unstable steady solution corresponding to the lower branch bifurcates into a time-

periodic solution, while the unstable solution corresponding to the loop bifurcates into the steady upper-branch solution. Hence theory predicts that as the wavenumber increases a discontinuity arises in the solution which shifts from the steady upper-branch behaviour to the time-periodic behaviour bifurcating from the lower branch.

That two different types of behaviour should arise below and above resonant conditions is not surprising, though this does not seem to have been recognized before. Indeed the same behaviour is exhibited by the linear forced solution described in §3, the branch of solution with $\lambda > \lambda_R$ being unstable. In fact free migrating bars do not amplify below resonance (hence no homogeneous solution of the linear unsteady problem exists), but they are unstable when $\lambda > \lambda_R$. Hence under the latter conditions the linearly unstable homogeneous part of the solution interacts nonlinearly with the steady forced part giving rise to the time-periodic pattern detected numerically. As a result of the above nonlinear interaction the bifurcation into a time-periodic solution is shifted toward values of wavenumber larger than λ_R, i.e. positive values of λ_1, as shown in figure 8(*a*). For the same reason a discontinuity arises in the solution of (56) in terms of the width ratio, for values of β slightly larger than β_R (see figure 8*b*).

Figure 9 allows a comparison between the weakly nonlinear resonant solution developed herein and the linear forced solution. Notice that in the plots only the contribution associated with the fundamental harmonic in the longitudinal direction e_1, i.e. the $O(\nu^{\frac{1}{3}})$ component of the nonlinear solution (49), has been kept. The figure shows that, rather than exhibiting a sharp peak within the resonant range, the system response follows a fairly smooth trend with a relatively weak maximum for values of meander wavenumber larger than the resonant value.

In other words, not only do nonlinear effects suppress the singularity exhibited by the linear solutions at $\lambda = \lambda_R$ but they also control the bed response within a fairly wide range of values of meander wavenumber whose amplitude depends on the values of curvature ratio ν through (49).

7. Nonlinear resonance and bend instability

Before we compare the above results with experimental observations we first analyse how the effects of nonlinearity close to resonance affect the formulation and the predictions of a bend instability theory.

Indeed such reflections are needed since we are confronted with a fairly peculiar stability problem where the most unstable perturbations also coincide with resonant perturbations so that the order of magnitude of the excitation does not coincide with the order of magnitude of the response of the system. In other words the stability problem will be seen to be intrinsically nonlinear.

A bend stability theory can be formulated by associating a bank equation with the governing equations for flow and bottom topography. Attempts to describe in some detail the mechanics of bank erosion have been proposed in the recent literature (Hasegawa 1989; Mosselman 1989). All of them are based on steady models of the process, neglecting its character which is known to be intermittent in nature (Nanson & Hickin 1983). Furthermore they all assume bank erosion to be associated with some measure of the near-bank flow perturbation induced by curvature, thus assuming that the channel cross-section would otherwise be in equilibrium. The work of Parker (1978) suggests that under bedload-dominated conditions the latter requirement implies that the average Shields stress must exceed the critical value by

a small amount. A second implication of the above models is that some other mechanism must exist to allow for the accretion of the convex bank such as to keep the channel width constant while the concave bank is progressively eroded. This mechanism is related to sediment deposition; however, its details have never been investigated and will require elucidation. A third basic assumption of bend theories is that the rate of bank erosion must be much smaller than the characteristic speed of alternating bars. This assumption may well hold under field conditions but is usually not met in the laboratory: this invariably leads to the eventual development of a braided stream in laboratory experiments. In other words the 'bend' approach is likely to describe more appropriately the actual phenomenon occurring in the field rather than that reproduced in model experiments. A further assumption of bend theories is that the influence of previously formed free bars is neglected, although there exists experimental evidence suggesting that bend instability proceeds after migrating bars have already undergone a finite-amplitude development. A quantitative description of the above influence is given in Seminara & Tubino (1989).

It is outside the scope of the present paper to attempt setting firmer foundations of bend stability theory. We are, rather, interested in this section in ascertaining how classical bend theories can accommodate the effects of flow nonlinearities close to resonance. Hence we simply follow an approach similar to that originally proposed by Ikeda *et al.* (1981) and write the bank erosion equation in the form

$$\cos(\sigma)\frac{\partial y^*}{\partial t^*} = E\{(U^*)_{n^*=B^*} - (U^*)_{n^*=-B^*}\}. \tag{63}$$

In (63) $y^*(x^*, t^*)$ is the transverse Cartesian coordinate of the channel axis measured with respect to a Cartesian longitudinal axis x^* (see figure 1), $\sigma(x^*, t^*)$ is the angle between the local direction of the channel axis and the x^* axis, and E is an erosion coefficient. It should be noticed that components of flow perturbations which are symmetric in the transverse direction may induce bank erosion but do not lead to any lateral shift of the channel axis. In order to account for this feature the flow property assumed to induce bank erosion is taken to be the difference between the values attained by perturbations of longitudinal velocity at the two banks. We also point out that the work of Parker (1978) on the equilibrium shape of the cross-section of gravel rivers, where it is shown that equilibrium is not incompatible with sediment transport, would suggest that the perturbation of some measure of bank stress rather than of near-bank velocity is presumably a more appropriate quantity to associate with the rate of bank retreat. However, since alternative choices of any specific near-bank property do not alter the qualitative features of the process we want to analyse, we keep the assumption (63) which corresponds to the one originally proposed by Ikeda *et al.* (1981) and has also received some support from the recent work of Hasegawa (1989).

In order to use results of nonlinear resonant meander theory it is necessary to write (63) in intrinsic coordinates. Recalling (1) and (4) and allowing for meander growth and migration we can write

$$\frac{\mathrm{d}\sigma}{\mathrm{d}s} = -\nu(t)\{\exp[\mathrm{i}\lambda(\nu)(s-\phi(t))] + \text{c.c.}\}, \tag{64}$$

where the intrinsic meander wavenumber λ and the meander wave speed $c \equiv \phi_{,t}$ do vary during meander growth; hence, they are in general functions of dimensionless curvature ν.

From (64) one readily finds

$$\sigma = \mathrm{i}\frac{\nu}{\lambda}\exp\left[\mathrm{i}\lambda(s-\phi)\right]+\text{c.c.}, \tag{65}$$

hence

$$y = \frac{\nu}{\lambda^2}\exp\left[\mathrm{i}\lambda(s-\phi)\right]+\text{c.c.}+O\left(\frac{\nu^3}{\lambda^4}\right) \tag{66}$$

and

$$\lambda = \lambda_x\left[1-\frac{\nu^2}{\lambda_x^2}+O\left(\frac{\nu}{\lambda_x}\right)^4\right], \tag{67}$$

where y is y^* scaled by B^* and λ_x is the dimensionless Cartesian meander wavenumber. From (67) it follows that, as long as (ν/λ_x) remains small, as a first approximation we can take λ to be constant and equal to λ_x. Furthermore (65) implies that $\cos(\sigma)$ can be approximated by 1, neglecting the contribution of order $(\nu/\lambda_x)^2$. The dimensionless form of (63) then becomes

$$y_{,t} = \frac{E}{Q_0}(U|_{n=1}-U|_{n=-1}). \tag{68}$$

Since the parameter E/Q_0 is usually small, the rate of bend development being of the order of metres/year (hence $E \sim 10^{-7}$–10^{-8}) with Q_0 ranging between 10^{-3} and 10^{-5}, the adjustment of flow and bed topography to the planimetric development of the channel axis can be taken to occur instantaneously at the timescale of the latter and (68) can be decoupled from the governing equations of flow and bed topography.

If we follow the latter procedure, substitute from (66) into (68) and use for U the solution in the form (49) with $(\lambda_{\mathrm{R}} s)$ replaced by $[\lambda_x^{\mathrm{R}}(s-\phi)]$ (λ_x^{R} being the resonant Cartesian wavenumber), we find

$$(\nu_{,t}-\mathrm{i}\lambda_x^{\mathrm{R}}\nu c) = \left[2\frac{E}{Q_0}(\lambda_x^{\mathrm{R}})^2 A_{\mathrm{e}} u_1^{\mathrm{R}}\right]\nu^{\frac{1}{3}}. \tag{69}$$

Integration of the real and imaginary parts of (69) then gives

$$\nu = \left[\frac{4}{3}\frac{E}{Q_0}(\lambda_x^{\mathrm{R}})^2\,\mathrm{Re}\,(A_{\mathrm{e}} u_1^{\mathrm{R}})\right]t^{\frac{3}{2}}+\nu_0, \quad c = \left[-2\frac{E}{Q_0}\lambda_x^{\mathrm{R}}\,\mathrm{Im}\,(A_{\mathrm{e}} u_1^{\mathrm{R}})\right]\nu^{-\frac{2}{3}}, \tag{70a, b}$$

with ν_0 the initial amplitude of the perturbation of channel curvature. Calculations show that at resonance $\mathrm{Re}\,(A_{\mathrm{e}} u_1^{\mathrm{R}})$ is positive and $\mathrm{Im}\,(A_{\mathrm{e}} u_1^{\mathrm{R}})$ is negative both in the plane and in the dune cases, hence instability does indeed occur with positive values of the meander wave speed.

The above results deserve some comments. The nonlinear character of the resonant response of bed topography to the forcing effect of curvature leads to the growth rate $\nu_{,t}$ being proportional to $\nu^{\frac{1}{3}}$ rather than ν, which implies an algebraic rather than exponential growth of channel curvature. Furthermore, meander wave speed is found to decrease as curvature increases, which corresponds to physical expectation.

We point out that a singular behaviour of c is predicted by (70) at $t = 0$ as $\nu_0 \to 0$. However as $\nu_0 \to 0$ the timescale of meander growth becomes comparable with the timescale of evolution of bottom topography. This is readily seen. Indeed if we define

$$T = \nu_0^{\frac{2}{3}} t, \quad \nu = \nu_0 N(T), \tag{71a, b}$$

the amplitude function A reaches the equilibrium amplitude A_{e} through a transient process described by the time variable T. Hence for values of ν_0 small enough for the relationship

$$E/Q_0 = e\nu_0^{\frac{4}{3}} \tag{72}$$

to hold with $e \sim O(1)$, equation (70*a*) is no longer valid and the bank erosion equation for $N(T)$ and the evolution equation for $A(T)$ are coupled. As ν increases, meander development tends to the algebraic growth predicted by the decoupled solution (70).

In the above discussion we have taken the view typical of classical bend stability theories where the channel topography is initially disturbed only by an infinitesimal perturbation of channel curvature. The analysis would need modification to accommodate the effects of spatial bars if they are initially present in the originally straight channel. In this case, which corresponds to the viewpoint of the Dutch school, the perturbations forcing bank erosion are independent of curvature so that the bank erosion equation (69) predicts a linear growth of ν in the initial stage of meander development. As ν has grown large enough for the relationship

$$\nu^{\frac{1}{3}} \sim O(\beta - \beta_R)^{\frac{1}{2}} \tag{73}$$

to hold, spatial bars essentially become forced bars and their amplitude is affected by curvature according to (55), (56). At this stage meander growth proceeds according to the algebraic behaviour described by (70) and already discussed.

8. Comparison with experimental results of Colombini, Tubino & Whiting (1990)

The main achievement of the present work appears to be the suggestion that the prediction of bed topography in meandering channels characterized by near-resonant conditions requires the use of nonlinear models since resonance operates in a form which is markedly different from that predicted by linear analyses as shown in figure 9.

The possible impact of these results on the problem of modelling river dynamics seemed to dictate the importance of a detailed and systematic laboratory experiment able to check the actual correspondence between theoretical model and physical reality. These experiments were carefully designed and performed in the fluvial laboratory of the Hydraulic Institute of the University of Genoa by Colombini *et al.* (1990). The reader is referred to the latter paper for a detailed description and discussion of the experimental procedure. Here we briefly summarize the main results to allow some comparison with our theoretical findings.

Each experiment was performed by constructing a sinuous channel consisting of at least 3.5 meanders, with the channel axis following a sine curve. The values of the curvature ratio ν, the average slope S and the grain size d_s^* were kept constant through all the experiments, while the channel wavenumber and the width ratio were varied in a range as broad as possible close to the resonant values. The value of ν chosen was 0.05 as a compromise between the requirements of ν being large enough for suppression of migrating bars and small enough for the perturbation approach to be valid. This value of ν corresponds to natural meanders in the initial–intermediate stage of development. The values of S and d_s^* were 0.006 and 0.76 mm respectively, while the Cartesian wavenumber λ_x ranged between 0.15 and 0.30, and the values of the width ratio β fell in the range from 11 to 20. Notice that conditions were sought that would avoid the presence of small-scale bedforms (ripples, dunes) which might have made the interpretation of results in the light of present theory less reliable.

The typical output of each experiment was the development of an equilibrium configuration of the forced bars, sometimes disturbed by small propagating sand waves seen to be born within the pool at the concave bank and vanish downstream.

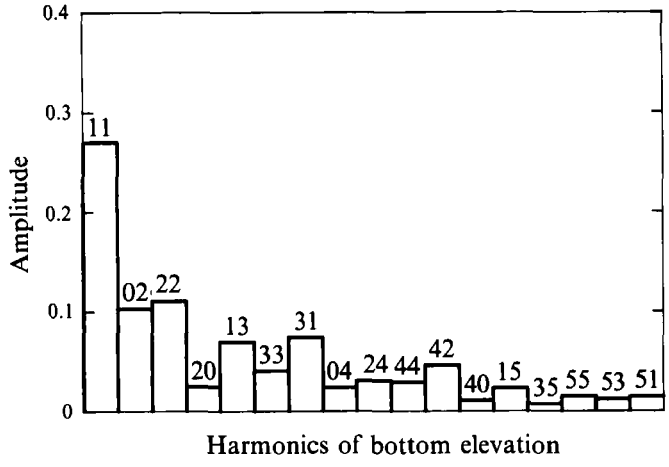

FIGURE 10. The main harmonics of the Fourier spectrum of bed elevation of run W25Q14 of Colombini *et al.* (1990). The amplitude of harmonics is given as percentage of the total. The first and second indexes reported on the abscissa refer to the longitudinal and transverse directions respectively.

For the smallest wavenumber ($\lambda_x = 0.15$) migrating alternate bars were also detected, whose amplitude was smaller than that of the fixed bars. Bed topography was preserved at the end of each experiment and measured with a laser scanner device, with a precision of 0.01 mm, driven by a stepper motor and run by a personal computer.

A useful operation performed by Colombini *et al.* (1990) on the experimental data was a two-dimensional Fourier analysis which allowed the contribution of the various harmonics in the longitudinal and transverse directions to be identified. Figure 10 shows a typical spectrum of the amplitudes of bottom harmonics as found by Colombini *et al.* (1990). This plot clearly supports the weakly nonlinear structure of the response of bed topography in that the fundamental 11 harmonic plays the most important role while higher harmonics are present which appear to be generated by a cascade process showing intensities which do decay as the order of the harmonics increases. It should be noticed that in general the fundamental 11 harmonic is found to only account for 15–30% of the total spectrum of bottom topography. Moreover, the intensity of second harmonics (22, 02, 20) is about one-third of the intensity of the fundamental. These findings can be taken as strong, though indirect, evidence that a nonlinear resonance effect was indeed operating in the experimental process. In fact in the absence of resonance a straightforward perturbation scheme in integer powers of ν would predict a much faster decay of the intensity of higher harmonics produced by nonlinear interactions: at each order m the intensity should be $O(\nu)$ smaller than the intensity of harmonics of order $(m-1)$. Hence in Colombini *et al.*'s (1990) experiments one would expect second-order harmonics to have an intensity of about 5% of the intensity of the fundamental, which is very far from observations.

Once the weakly nonlinear structure of the solution and its resonant character has been confirmed the question arises of what comparison between theory and experiments is most appropriate. Indeed the experimental results suggest that the overall contribution of fundamental and second harmonics, which are the only ones derived in the present theory, only account for about 50–60% of the total 'energy'. Hence a detailed comparison is more appropriately performed between the behaviour

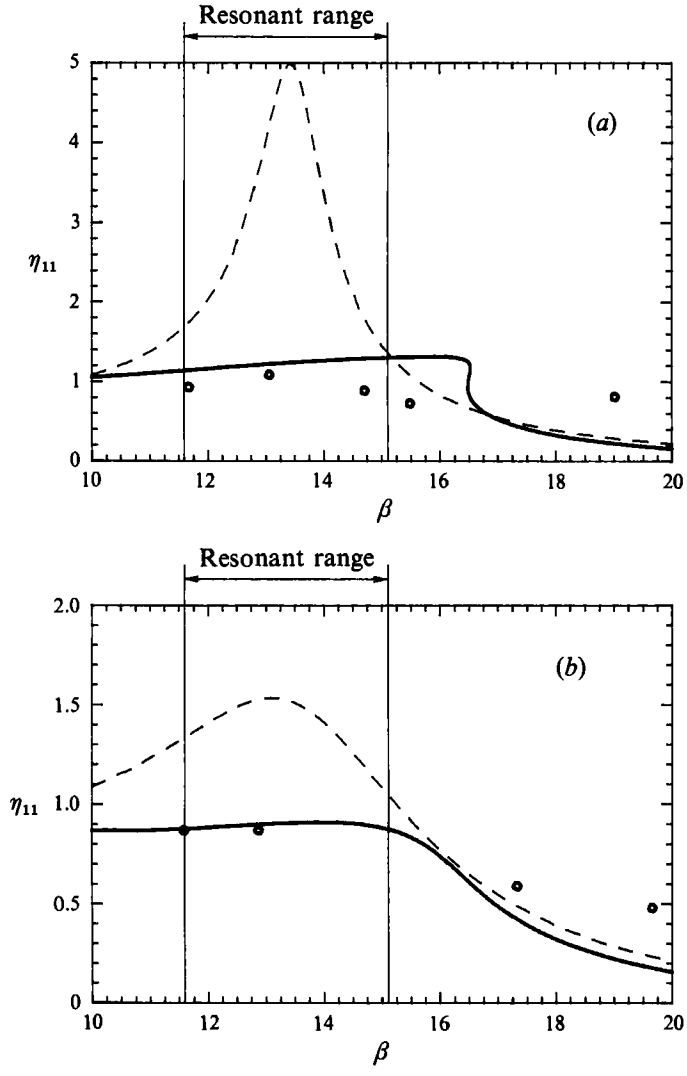

FIGURE 11. The dimensionless amplitude of the first harmonic of bottom elevation η_{11} as predicted by the present weakly nonlinear theory (solid curve) and by the linear theory (dashed curve) is plotted versus the width ratio of the channel β and compared with the experimental findings of Colombini *et al.* (1990) (○) for different values of meander wavenumber. The resonant range is defined by (48*a*) with $\beta_1 = \pm 1$. (*a*) $\lambda_x = 0.2$; (*b*) $\lambda_x = 0.15$.

of the various harmonics rather than between the overall results concerning bottom elevation.

In figure 11 (*a*, *b*) we compare the amplitude of the first harmonic of the solution for the bottom elevation as predicted by linear and weakly nonlinear theories with the values experimentally observed for the two set of experiments with λ_x equal to 0.2 and 0.15 respectively. For a given channel geometry and given values of channel width, average slope and grain sizes, a continuous curve which represents the predicted response of the bottom to variations of flow discharge changes can be drawn in terms of width ratio. The Shields stress θ_0 and roughness parameter d_s change accordingly along the theoretical curves plotted in figure 11. The comparison seems to be fairly satisfactory if account is taken of the fact that the weakly

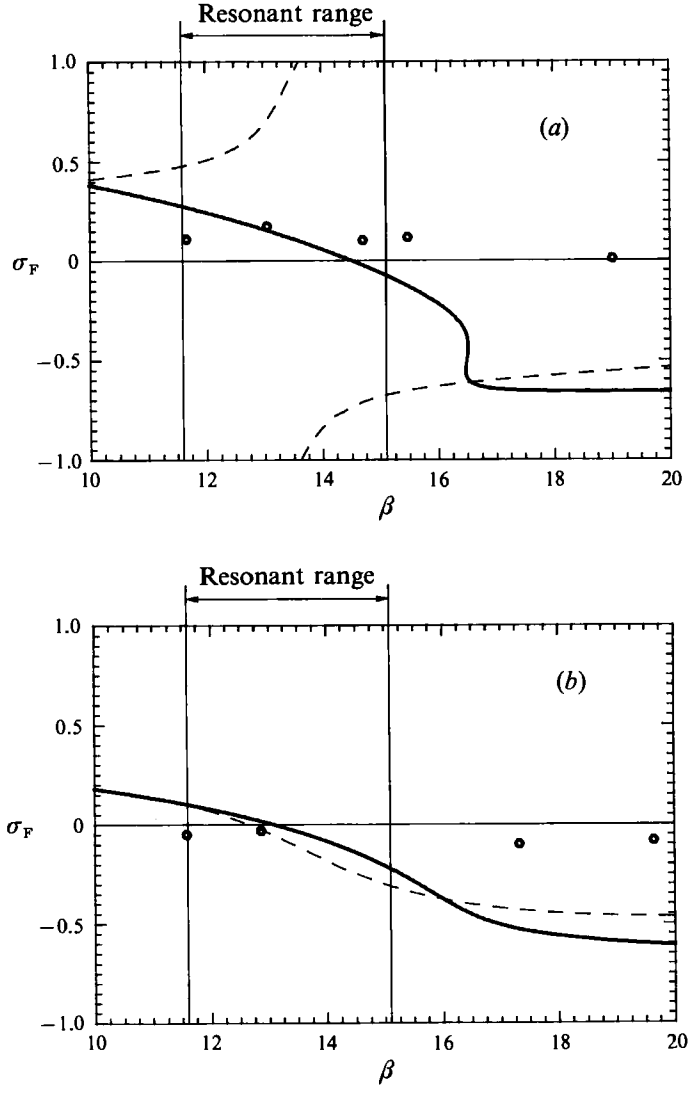

FIGURE 12. The phase shift σ_F of the scour hole with respect to the bend apex associated with the first harmonic as predicted by the present weakly nonlinear theory (solid curve) and by the linear theory (dashed curve) is plotted versus the width ratio of the channel β and compared with the experimental findings of Colombini *et al.* (1990) (○) for different values of meander wavenumber. The resonant range is defined by (48*a*) with $\beta_1 = \pm 1$. (*a*) $\lambda_x = 0.2$; (*b*) $\lambda_x = 0.15$.

nonlinear solution strictly applies only within a neighbourhood $O(\nu^{\frac{2}{3}})$ of the resonant values of λ and β (the resonant range reported in the figures). Notice that β_R is close to 13 and λ_R is in the range from 0.165 to 0.175 for values of Shields and roughness parameter typical of these experiments.

Similar comparisons for the position of the scour hole with respect to the bend apex are given in figure 12(*a*, *b*). The latter quantity is given in terms of the dimensionless parameter $\sigma_F = (\lambda_x \Delta x)/\pi$, with Δx dimensionless longitudinal distance from the bend apex of the position of maximum scour associated with the first harmonic, so that σ_F changes from negative to positive values as the scour hole shifts from upstream to downstream.

Figures 11 and 12 clearly show that the linear theory provides quite poor predictions in a fairly wide range close to resonance.

We do not pursue in detail comparisons for the second harmonics. It suffices here to state that weakly nonlinear theory overestimates the overall contribution of second harmonics close to resonance by a factor of roughly 20%. Furthermore the intensities of the various second harmonics are not uniformly distributed but show a peak in the 22 harmonic. This is not in agreement with experimental observations.

The latter discrepancy is most likely because the experimental value of ν nonlinearity is not quite as weak as our theory would require. In fact notice that the amplitude $|A_e|$ attains values of about 2–3, hence $\nu^{\frac{1}{3}}|A_e|$ falls in the range from 0.85 to 1.15. Intensities of higher harmonics do exhibit a decreasing trend because coefficients in the expansion are found to decrease with increasing order. However, the effect of higher-order terms on the low-order harmonics cannot be assumed quite negligible as assumed in the weakly nonlinear approach.

To overcome the above deficiencies one should resort to a fully nonlinear spectral solution of the problem of the type obtained by Colombini & Tubino (1990) for the case of migrating free bars in straight channels.

9. Discussion

Let us finally summarize and discuss our main results.

The theory developed in §§4 and 5 shows that the structure of forced bars in a neighbourhood of resonant conditions is related to that of spatial 'free' bars in the sense that spatial bars 'deformed' by curvature develop in near-resonant meanders or, alternatively, spatial bars initially present in the straight channel configuration are deformed by curvature as meandering develops. Mathematically, curvature provides a forcing term in the equilibrium-amplitude equation of forced bars which would otherwise be identical to the equation governing 'free' spatial bars.

We have also shown that the effects of nonlinearity damp the infinite peak in the response of resonant meanders. Furthermore, the effects of resonance are felt within a range which widens, as ν increases, like $\nu^{\frac{2}{3}}$. Within this range the linear response is obviously markedly different from the nonlinear one. These findings are based on a weakly nonlinear analysis valid in a neighbourhood of the resonant conditions. How far from resonance its validity can be extended is an important question which will require elucidation based on strongly nonlinear numerical solutions of the type recently developed by Colombini & Tubino (1990) for free migrating bars.

A related question is that of ascertaining the significance of the non-uniqueness of the solution of the amplitude equation in the form (56). This feature always occurs, but the corresponding range of values of λ is found to fall increasingly far from resonance as ν increases. Hence when ν is large enough for the present theory (which ignores the coexistence of migrating free bars with forced bars) to hold, the loop occurs relatively far from resonance where the validity of our weakly nonlinear approach must be questioned. Physically one would expect a discontinuity in the response of channel topography as λ varies. This feature has not been detected in Colombini *et al.*'s (1990) experiments. However, in order to infer that a non-unique response does not actually occur we would need a wider range of experiments and the results of fully nonlinear calculation valid for large values of λ. This is matter for future research.

We have also reconciled, through the analysis of §7, the intrinsic nonlinearity of the near-resonant channel response with the bend stability approach. It may be of

some interest to point out that nonlinear resonance also provides a mechanism able to excite third harmonics of channel curvature much faster than one would expect in the absence of resonance. Third harmonics are often present in mature meanders leading to their characteristic fattening and skewing first revealed by Kinoshita (1961).

Parker *et al.* (1983) have analysed the possible existence of trains of bends of permanent form whose shape was characterized by a sine-generated curve plus third harmonics of smaller amplitude. The latter work was based on a linear model for flow and bed topography; hence it neglected 'flow' nonlinearities but preserved 'geometric' nonlinearities. The present theory helps understanding how 'geometric' nonlinearities are generated. In fact the bank erosion equation suggests that the latter are forced by the cascade of higher harmonics of near-bank velocity whose amplitude decays as their order increases. In other words, 'flow' nonlinearities generate 'geometric' nonlinearities: in particular the rate of growth of third harmonics is $O(\nu)$ in near-resonant conditions while it remains much smaller, $O(\nu^3)$, far from resonance. Again one would hardly expect the latter intensity to be strong enough to actually develop geometric nonlinearities and this seems to support the idea that finite-amplitude bends do develop from near-resonant conditions.

Hence the main geomorphological implication of the present work is the explanation of the generation mechanism of the characteristic fattening and skewing typical of mature meanders.

Several features of the problem will require further attention in the future. Firstly, as previously pointed out, experimental observations show that the overall effect of harmonics higher than the second is significant. This is hardly surprising since the near-resonant expansion involves $\nu^{\frac{1}{3}}$ as a small parameter, which implies a fairly slow decay of the amplitudes of higher harmonics. A full numerical, possibly spectral, solution of the problem is required if quantitatively accurate results are sought. The latter will also allow the actual structure of the solution in the ranges corresponding to the loop and the lower branch of the weakly nonlinear steady solution to be ascertained.

The present results strongly suggest that the literature on flow and bed topography in meandering channels based on linear theories needs to be revisited. Indeed for fairly small channel curvatures free bars coexist with forced bars and interact nonlinearly as discussed in TS. As curvature exceeds the threshold value for free-bar suppression steady forced bars keep a nonlinear near-resonant structure within a fairly wide range of values of wavenumber and width-to-depth ratio.

A second extension of the present work is required. For small enough values of ν migrating free bars are not suppressed. Tubino & Seminara's (1990) work on free-bar suppression employed a linear theory for forced bars also in the resonant range. A modification of the latter analysis is required in a neighbourhood of resonance. This would provide a complete description of flow and bed topography in a regular sequence of near-resonant meanders.

A third obvious development of the present work would be achieved by calculating third-order effects in our near-resonant expansion, a calculation which is still analytically feasible. This would allow our knowledge of flow and bed topography to be incorporated into the framework of a bend stability theory able to predict the development of Kinoshita's curve.

Various other questions still await an answer. In particular, what is the mechanism which controls the formation of multiple bars in tortuous meanders? A possible line to attack this problem might be to analyse whether the periodic pattern associated

with a regular sequence of meanders might be subject to some kind of ultraharmonic Mathieu instability. Furthermore, what is the origin of irregularity of meander patterns observed in nature? Is it related to non-uniformity of local environmental conditions as suggested in the geomorphological literature or is it inherent in the deterministic behaviour of rivers as nonlinear dynamical systems? This question calls for the modelling of tortuous meanders, a still open subject. Its investigation would also hopefully allow one to understand the reduction of meander growth rate observed for large-amplitude meanders (Nanson & Hickin 1983).

Finally, among the various simplifying assumptions embodied in our formulation, two seem to warrant particular attention in future research: neglect of suspended load and of the unsteady, intermittent, character of meander development.

This work was supported by MURST (Italian National Research Projects). Part of this work was completed while the senior author (G.S.) was visiting St. Anthony Falls Hydraulics Laboratory. The interest of G. Parker in this work, his financial support and several exciting discussions are gratefully acknowledged. We are also grateful to M. Colombini and P. Whiting for providing their experimental data for comparison with the present theoretical results. Short preliminary versions of parts of the present results were presented at the IAHR Workshop on Mountain Rivers (Trento, 1989) and at the XXII Convegno di Idraulica e Costruzioni Idrauliche (Cosenza, 1990).

REFERENCES

BLONDEAUX, P. & SEMINARA, G. 1985 A unified bar-bend theory of river meanders. *J. Fluid Mech.* **157**, 449–470.

CHIEN, N. 1956 The present status of research on sediment transport. *Trans. ASCE* **121**, 833–868.

CODDINGTON, E. A. & LEVINSON, N. 1955 *Theory of Ordinary Differential Equations*. McGraw-Hill.

COLOMBINI, M., SEMINARA, G. & TUBINO, M. 1987 Finite-amplitude alternate bars. *J. Fluid Mech.* **181**, 213–232 (referred to herein as CST).

COLOMBINI, M. & TUBINO, M. 1990 Finite amplitude free-bars: a fully nonlinear spectral solution. In *Sand Transport in Rivers, Estuaries and the Sea* (ed. R. Soulsby & R. Bettes). *Proc. Euromech 262 Colloquium, Wallingford, UK, 26–29 June*, pp. 163–169. Balkema.

COLOMBINI, M., TUBINO, M. & WHITING, P. 1990 Topographic expression of bars in meandering channels. In *Dynamics of Gravel-Bed Rivers* (ed. P. Billi, R. D. Hey, C. R. Thorne & P. Tacconi), pp. 457–474. Wiley & Sons.

ENGELUND, F. 1974 Flow and bed topography in channel bends. *J. Hydraul. Div. ASCE* **100** (HY11), 1631–1648.

ENGELUND, F. & HANSEN, E. 1967 *A Monograph on Sediment Transport in Alluvial Streams*. Copenhagen: Danish Technical Press.

FERGUSON, R. I. 1975 Meander irregularity and wavelength estimation. *J. Hydrol.* **26**, 315–333.

HASEGAWA, K. 1989 Studies on qualitative and quantitative prediction of meander channel shift. In *River Meandering* (ed. S. Ikeda & G. Parker). AGU Water Resources Monograph, vol. 12, pp. 215–235.

IKEDA, S. 1982 Lateral bedload transport on sides slopes. *J. Hydraul. Engng ASCE* **108**, 1369–1373.

IKEDA, S., PARKER, G. & SAWAI, K. 1981 Bend theory of river meanders. Part 1. Linear development. *J. Fluid Mech.* **112**, 363–377.

JOHANNESSON, H. & PARKER, G. 1989 Linear theory of river meanders. In *River Meandering* (ed. S. Ikeda & G. Parker). AGU Water Resources Monograph, vol. 12, pp. 181–213.

KALKWIJK, J. P. TH. & VRIEND, H. J. DE 1980 Computation of the flow in shallow river bends. *J. Hydraul. Res.* **18**, 327–342.

KINOSHITA, R. 1961 Investigation of channel deformation in Ishikari River. *Rep. Bureau of Resources, Dept. Science & Technology, Japan*, pp. 1–174.

LANGBEIN, W. B. & LEOPOLD, L. B. 1966 River meanders-theory of minimum variance. *USGS Professional Paper* 422H, pp. 1–15.

MOSSELMAN, E. 1989 Theoretical investigation on discharge-induced river bank erosion. *Commun. Hydraul., Delft University of Technology Rep.* 3–89.

NANSON, G. C. & HICKIN, E. J. 1983 Channel migration and incision on the Beatton river. *J. Hydraul. Engng ASCE* **109**, 327–337.

ODGAARD, J. A. 1989 River-meander model. I: Development. *J. Hydraul. Engng ASCE* **115**, 1433–1450.

OLESEN, K. W. 1983 Alternate bars and meandering of alluvial rivers. *Commun. Hydraul., Delft University of Technology Rep.* 7–83.

PARKER, G. 1978 Self-formed straight rivers with equilibrium banks and mobile bed. Part 1. The gravel river. *J. Fluid Mech.* **89**, 127–146.

PARKER, G. 1984 Discussion of: 'Lateral bedload transport on side slopes' by S. Ikeda. *J. Hydraul. Engng ASCE* **110**, 197–199.

PARKER, G., DIPLAS, P. & AKIYAMA, J. 1983 Meander bends of high amplitude. *J. Hydraul. Engng ASCE* **109**, 1323–1337.

ROZOVSKII, I. L. 1957 *Flow of Water in Bends of Open Channels.* Kiev: Acad. Sci. Ukhranian SSR.

SEMINARA, G. 1989 River bars and nonlinear dynamics. In *Proc. IAHR Workshop on Fluvial Hydraulics of Mountain Regions, Trent, Italy, 3–6 October.*

SEMINARA, G. & TUBINO, M. 1985 Further results on the effect of transport in suspension on flow in weakly meandering channels. In *Colloq on The Dynamics of Alluvial Rivers*, pp. 67–112. Hydraulic Institute, Genoa University.

SEMINARA, G. & TUBINO, M. 1989 Alternate bars and meandering: free, forced and mixed interactions. In *River Meandering* (ed. S. Ikeda & G. Parker). AGU Water Resources Monograph, vol. 12, pp. 267–320.

SEMINARA, G. & TUBINO, M. 1991 Discussion of: 'River-meander model. I: Development'. By J. A. Odgaard, *J. Hydraul. Engng ASCE* **117**, 1088–1091.

STRUIKSMA, N. & CROSATO, A. 1989 Analysis of a 2-D bed topography model for rivers. In *River Meandering*, (ed. S. Ikeda & G. Parker). AGU Water Resources Monograph, vol. 12, pp. 153–180.

STRUIKSMA, N., OLESEN, K. W., FLOKSTRA, C. & VRIEND, H. J. DE 1985 Bed deformation in curved alluvial channels. *J. Hydraul. Res.* **23**, 57–79.

THOMPSON, J. M. T. & STEWART, H. B. 1986 *Nonlinear Dynamics and Chaos.* Wiley & Sons.

TUBINO, M. & SEMINARA, G. 1990 Free–forced interactions in developing meanders and suppression of free bars. *J. Fluid Mech.* **214**, 131–159 (referred to herein as TS).